15 (2022) 100156

Contents lists available at ScienceDirect

International Journal of Thermofluids

journal homepage: www.elsevier.com/locate/ijtf

A comparison of axial turbine loss models for air, sCO_2 and ORC turbines across a range of scales

Salma I. Salah *, Martin T. White, Abdulnaser I. Sayma

Thermo-Fluids Research Centre, Department of Engineering, City, University of London, Northampton Square, London, EC1V 0HB, United Kingdom

ARTICLE INFO

Keywords:
Performance analysis
Non-conventional working fluids
Loss models
Air turbines
sCO_2 turbines
ORC turbines

ABSTRACT

Loss models are used to evaluate the aerodynamic performance of axial turbines at the preliminary design stage. The commonly used loss models were derived for air and steam turbines and have not been sufficiently investigated for turbines working with non-conventional working fluids, relevant to new power systems, such as organic fluids and supercritical CO_2 (sCO_2). Thus, the aim of this study is to explore the deviation between the performance predictions of different loss models, namely Dunham and Came, Kacker and Okapuu, Craig and Cox and Aungier, for non-conventional working fluids where turbines may differ in design and operation than conventional air or steam turbines. Additionally, this paper aims to investigate the effect of the turbine scale on the trends in the performance predictions of these models. Three different case-studies are defined for air, organic Rankine cycle (ORC) and sCO_2 turbines and each one is evaluated at two different scales. It is found that the selected loss models resulted in varying loss predictions; particularly for predicting the losses due to the clearance gap for all small scale designs. Furthermore, large variations were found in predicting the effect of the flow regime on the turbine performance for all models.

1. Introduction

Axial turbines are extensively installed in power generation and propulsion systems due to their capability of handling high mass-flow rates efficiently along with accommodating multiple expansion stages on a single shaft. Preliminary aerodynamic turbine design and optimisation is a necessary step within the turbine design process that precedes advanced 3D blade optimisation and flow analysis studies using computational fluid dynamics (CFD). Throughout the preliminary design phase, turbine performance is estimated by quantifying the energy losses that the working fluid experiences during the expansion in the stator and rotor blade rows. In this regard, aerodynamic losses can be classified into profile, secondary flow, tip clearance and trailing edge losses. Several mathematical correlations have been developed to quantify these losses within axial turbines including correlations proposed by Soderberg (SB) [1], Ainley and Mathieson (AM) [2], Craig and Cox (CC) [3], Dunham and Came (DC) [4], Kacker and Okapuu (KO) [5] and eventually Aungier (AN) [6].

All of these existing models have been derived and validated for air and steam turbines, and have shown a good agreement with experimental data with a maximum efficiency deviation of 3% reported for the AM model [2]. In the meantime, organic Rankine cycles (ORC) are being widely considered for low- to medium-temperature applications (<400 °C) including waste-heat recovery, solar-thermal and geothermal [7]. Furthermore, closed loop super-critical carbon dioxide (sCO_2) power cycles are promising candidates for concentrated-solar power, nuclear and waste-heat recovery applications, having advantages of compact turbomachinery offering a simple layout, high-power density and compact structures and high cycle efficiencies at heat-source temperatures in the range of 400 to 800 °C [8]. Within these new applications the required turbine designs may differ significantly from air or steam turbines; sCO_2 turbines experience several challenges due to the compact geometries, high density and low viscosity working fluid compared to air turbines which results in high clearance, windage losses and large frictional losses, whilst ORC turbines are characterised by low enthalpy drop (for a defined pressure ratio compared to air), and low speed of sound which leads to large volumetric expansion ratios and supersonic flow.

To date there has been limited experimental data to provide sufficient validation that existing turbine models are suitable for these non-conventional working fluids. However, despite this, several researchers have applied these models to the design of axial turbines for ORC and sCO_2 systems.

Lee et al. [9] implemented the mean-line design methodology for a sCO_2 axial turbine design, and refined it with Balje and Binsley [10]

* Corresponding author.
E-mail address: salma.salah.2@city.ac.uk (S.I. Salah).

https://doi.org/10.1016/j.ijft.2022.100156
Received 28 February 2022; Received in revised form 29 April 2022; Accepted 30 April 2022
Available online 14 May 2022

Table 1
Summary of the commonly used loss models for non-conventional turbine designs from the literature.

Study	Loss model	Working fluid	Scale [MW]
Lee et al. [2012] [9]	Balje and Binsley [10] & Kacker and Okapuu [5]	sCO_2	–
Schmitt et al. [2014] [11]	Soderberg [1]	sCO_2	100
Lio et al. [2014] [13]	Aungier [6]	Organic fluid	0.43
Meroni et al. [2016] [18]	Craig and Cox [3]	Organic fluid	–
Lio et al. [2016] [15]	Aungier [6]	Organic fluid	–
Talluria et al. [2017] [14]	Aungier [6]	Organic fluid	–
Meroni et al. [2018] [17]	Craig and Cox [3]	Organic fluid	–
Agromayor et al. [2019] [16]	Kacker and Okapuu [5]	Organic fluid	0.25,5
Salah et al. [2020] [12]	Soderberg [1]	sCO_2	0.1

and Kacker and Okapuu loss correlations to analyse the turbine performance; where the model results have shown a good agreement with experimental data [9]. Schmitt et al. [11] and Salah et al. [12] employed Soderberg's model [1] to design the first stage of 100 MW and 100 kW sCO_2 turbines respectively [12]; where the model was found to be insufficient for evaluating the performance of the 100 MW sCO_2 turbine.

With regards to ORC applications, Lio et al. [13] and Talluria et al. [14] examined the performance of an axial ORC turbine adopting Aungier [6] loss correlations. New efficiency charts were produced using the selected model for R245fa and *n*-hexane respectively operating at different design conditions. In a different study, Lio et al. [15] implemented the same loss model to predict turbine performance for different ORC working fluids and examine the effect of fluid characteristics on the turbine performance maps. Agromayor et al. [16] examined the performance of an axial flow ORC turbine using Kacker and Okapuu [5] model where the model was validated against experimental data and a maximum efficiency difference of 2.07% was observed. Similarly, Meroni et al. [17] implemented Craig and Cox loss model correlations for the design of an ORC axial turbine and the model achieved a maximum efficiency difference of 1.3% in comparison to the verification cases. Additionally, Meroni et al. [18] implemented the same model to optimise the performance of an ORC turbine. A summary of the commonly used loss models for non-conventional turbine designs from the literature is presented in Table 1.

The first loss model for axial turbine design was developed back in 1949 by Soderberg [1] and one of the latest model updates was presented in 2006 by Aungier [6]. However, these models are still being used as part of the mean-line design procedure in recent studies as presented in Table 1. Specially, these models have been implemented in the design process of sCO_2 and ORC axial turbines within which each study has only applied a single loss model and considered a single working fluid, turbine scale or operating condition. Therefore, none of the previous studies have been able to highlight the discrepancies in the different models in predicting the turbine performance for non-conventional working fluids. Therefore, in the current study, a mean-line approach is adopted to investigate the behaviour of all the common loss models employed within the literature for different working fluids and turbine scales. The novelty in this current work lies in exploring the deviation between the performance predictions of the loss models, derived for air, for non-conventional working fluids. This information is considered an important contribution to the field as it aims to provide clarity on the selection of axial turbine loss models for application areas that are becoming increasingly important for future sustainable power production.

2. Selected case-studies

Three case-studies are defined for the assessment of the available loss models which relate to modern gas turbine, ORC and sCO_2 cycles. Steam and gas turbine systems have both been extensively studied and thus only a gas turbine case-study is considered as a comparison between turbines operating with conventional and non-conventional fluids.

In the current study, the operating conditions of General Electric's-Frame 9H four-stage turbine have been selected to represent a large-scale gas turbine [19]. Although, gas and steam cycles dominate in large-scale power generation applications, they are not considered to be the optimum option from low- to medium-temperature heat sources or applications with a limited power rating; here ORC cycles are attractive candidates [7,20]. The ORC cycle operating conditions are taken from one of the authors' previous works [21], which identified R1233zd(E), a modern hydrofluoroolefin with a low global-warming potential, as an optimal fluid for waste-heat recovery applications with heat-source temperatures in the region of 200 °C. Similarly, sCO_2 cycles are promising candidates for applications with heat-source temperatures in the range of 400 to 800 °C. Though the sCO_2 cycle efficiency is sensitive to the pressure ratios, the maximum pressure is limited due to the capital cost related to the piping and measurement systems and is typically around 20–25 MPa [22]. Therefore, the operating conditions of both the ORC and sCO_2 turbine have been set by the authors considering the above operational constraints [21,22] as detailed in Table 2.

Considering the above mentioned aspects, the case-studies listed in Table 2 have been selected to examine the performance of the various loss models for a range of operating conditions for three different working fluids (air, sCO_2 and R1233zd(E)) at two different turbine scales. In the present study, small-scale air, sCO_2 and ORC turbines are evaluated at shaft speeds of 89, 107 and 141 kRPM, corresponding to specific speeds of 0.25, 0.25 and 0.6 rad respectively, to avoid imposing high stresses on the rotor blades. However, synchronous designs with a rotational speed of 3000 RPM have been selected for the 100 MW sCO_2 and air designs to facilitate direct grid connection. The number of stages for air turbines is set to four, as specified in the literature [19]. Meanwhile, the number of stages for sCO_2 and ORC turbines are determined to allow for a gas bending stress within 10% of the maximum permissible bending stress; where the limit is specified based on previous experience. Similarly, the s/c ratio is varied among the various designs over the range from 0.5 and 1.1 [2] to allow for a feasible number of blades for each design case [23].

A mean-line axial turbine design approach is adopted and integrated with several loss models subroutines to provide an accurate estimation of the turbine performance for the selected case-studies. Within the model the steady-state mass, energy and momentum equations are solved to obtain the geometric parameters of the turbine. The same design methodology and steps detailed out in Ref. [12] have been adopted to obtain the design geometry across a turbine stage where constant enthalpy drop is assumed across each stage for multi-stage designs. The pressure loss coefficients for the stator and the rotor are obtained using correlations introduced in Ref. [3–6]. The pressure loss coefficients are converted to enthalpy loss coefficients from:

$$\zeta_N = Y_N \times \left(1 + 0.5(k\ M_2{}^2)\right) \tag{1}$$

$$\zeta_R = Y_R \times \left(1 + 0.5(k\ M_3{}^2)\right) \tag{2}$$

where k is the specific heat ratio, and M_2 and M_3 are the absolute rotor inlet and relative rotor outlet Mach numbers respectively. The total to total isentropic efficiency for each stage (η_{tt}) is then obtained from:

$$\eta_{tt} = \left[1 + \left(\frac{\zeta_R \frac{V_3^3}{2} + \frac{C_2^2}{2}\zeta_N \frac{T_3}{T_2}}{h_{01} - h_{03}}\right)\right]^{-1} \tag{3}$$

Table 2
Operating conditions for the selected case-studies.

Parameter	Description	Unit	Case-studies serial					
			C1 [19]	C2	C3	C4	C5	C6
–	Working fluid	[–]	Air		sCO_2		R1233zd(E)	
T_{01}	Total inlet temperature	[K]	1713.00		923.00		434.21	
P_{01}	Total inlet pressure	[MPa]	0.60		25.00		3.04	
PR	Pressure ratio	[–]	23.00		2.50		11.57	
n	Number of stages	[–]	4.00	4.00	8.00	6.00	2.00	
$\dot{m}$	Mass flow rate	[kg/s]	0.09	92.50	1.97	655.18	0.22	21.60
s/c	Pitch-to-chord ratio (1st stage)	[–]	1.10		0.80	0.60	1.10	
n_s	Specific speed	[rad]	0.25	0.33	0.25	0.13	0.60	0.60
N	Rotational speed	[kRPM]	89.40	3.00	106.90	3.00	141.10	14.10
$\dot{W}$	Power output	[MW]	0.10	100.00	0.30	100.00	0.01	1.00
k_s	Surface roughness	[mm]	0.002					
t_{cl}	Tip clearance gap	[mm]	0.400 (for large scale design)					

The mean-line design is then re-iterated using the updated enthalpy loss coefficients and estimate for stage efficiency with a convergence criterion less than 10^{-6} for both. This is completed for all the stages and the total turbine efficiency is obtained.

3. Key features for loss models and loss mechanisms

Within the existing loss models, Soderberg (SB) [1] introduced a set of simplified correlations for predicting profile and secondary flow losses in axial turbines in 1949. Following this Ainley and Mathieson (AM) [2] presented a method where the pressure losses were split into profile, secondary and tip clearance losses. Later, Craig and Cox (CC) [3] split the losses into profile, secondary and loss due to sudden enlargement in the flow path or wall cavity (annulus loss). Dunham and Came (DC) [4] later modified the performance correlations developed by AM using updated experimental data. The modifications considered profile, secondary and tip clearance losses. In a similar manner, additional modifications have been applied to the DC model by Kacker and Okapuu (KO) [5] and Aungier (AN) [6]. Alongside with the previously discussed losses, some of these models also accounted for other types of losses. For example, Craig and Cox considered other losses such as the leakage, disk windage, wetness and partial admission losses. Similarly, Aungier also considered lashing wire, leakage bypass, partial admission loss, disk friction and windage loss. For brevity, a full description of the loss correlations is provided in Appendix A.

In this study, losses are classified into profile, secondary, tip clearance, trailing edge, shock and supersonic expansion losses. Profile losses occurs due to the boundary layer effect where the fluid is subjected to viscous forces that slow down the flow and hence, increases the relative entropy in the mainstream. These forces might result in a wake formation, which is the region of disturbed flow downstream caused by the fluid flow around a solid body. Hence, profile losses can be in the form of friction losses, due to the fluid viscosity, on blade surfaces or losses in blade wakes. Secondary losses occurs due to the wall friction at tip and root of the blades along with the end-wall effects; the inlet boundary layer separates at the endwall of the blade, forming a horseshoe vortex as shown in Fig. 1(b). One leg of the vortex migrates to the pressure side (Fig. 1(a)) forming a vortex while the other move towards the suction side forming a counter vortex; the formed end-wall vortex secondary flow is responsible for the secondary flow losses. Trailing edge losses occurs due to the finite thickness of the trailing edge (Fig. 1(a)) at the blade which will result in flow separation at both the pressure and suction surfaces and create re-circulation zone. Tip clearance loss occurs due to the pressure difference between both blade sides, pressure and suction sides (Fig. 1(a)), along with the leakage over the tips of the blades

A brief overview of the various loss models is presented here to highlight the key components contributing to the estimated losses. Additionally, significant findings from the literature are presented to clarify the influence of key parameters such as Reynolds number and Mach number. This discussion is intended to provide a background for the predicted differences between loss models for both air and non-conventional working fluids across different scales.

The following loss models, including Ainley and Mathieson [2], Dunham and Came [4], Kacker and Okapuu [5] and Aungier [6], evaluated the flow losses based on the blade chord length. However, Craig and Cox [3] used the backbone (camber-line) length to evaluate the flow losses. Throughout the models' development process, several fluid flow phenomena have been considered including the characteristics of flow regime and fluid compressibility effects. Given that profile losses occur due to the formation of boundary layers on the blade surface, they are highly affected by Reynolds number, surface roughness, Mach number and trailing edge thickness. The effect of low Reynolds number (Re) has been previously investigated experimentally for air turbines [25–29] and it has been concluded that low Re results in an increase in both the size of the separation bubble and in the amount of flow separation. Moreover, it results in the development of secondary flows in the end wall region. Nonetheless, the effect of low Re has been found to be more significant on profile losses than on the secondary flow losses [25]. Reynolds number is evaluated based on the chord length for all models except for the CC model where it is evaluated based on the throat opening. Additionally, Reynolds number effects have been considered for both profile and secondary flow losses for the DC, CC and AN models, whilst the KO model considered it for only profile losses.

In view of the above effects, it is important to determine the critical Reynolds number where the transition from laminar to turbulent boundary layer occurs. Boundary layer transition is affected by the pressure gradient, free-stream Mach number and turbulence, and surface roughness. It has been found that the flow transition occurs at lower Re when the surface roughness height exceeds the critical roughness value. Though increasing Mach number reduces the transition Re, the critical roughness height is found to be greater for supersonic flows because of the Mach number effect on boundary layer thickness [30]. Accordingly, different critical Re have been set within loss models. The DC model evaluates the turbine performance at $Re = 2 \times 10^5$ and hence, a correction factor is applied when the Reynolds number deviates from the specified value. The AN model defines the transition region as $1 \times 10^5 < Re < 5 \times 10^5$ in comparison to $2 \times 10^5 < Re < 1 \times 10^6$ for the KO model, while the CC model defines a correction for Reynolds number effects for a wide range of Re with a correction factor of 1 at $Re = 1 \times 10^5$. The effect of surface roughness on the boundary layer thickness for turbulent flow has only been considered in the CC and AN models.

Besides the previous effects, as the flow accelerates adjacent to the curved leading edge, it experiences large oblique shock losses, due to fluid compressibility effects, and thus the inlet Mach number is recommended to be less than 0.6 [5]; where this effect is only

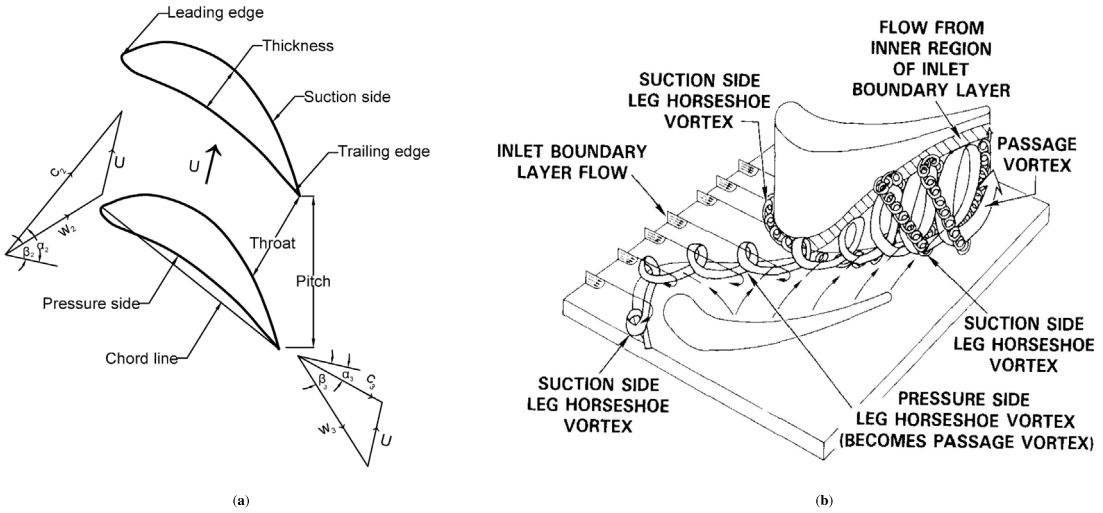

Fig. 1. (a) Geometry of a blade section (b) Endwall flow structure [24].

considered in the KO and AN models. Furthermore, reaching sonic flow conditions results in higher pressure losses occurring as a result of the normal shock wave originating at the trailing edge. This effect has been considered in the four loss models.

4. Model verification

Smith [31] provided a generalised chart to predict the efficiency of axial turbines considering various turbine geometries over a range of loading (ψ) and flow coefficients (ϕ), and hence it is widely used during mean-line design. The chart was developed for a four-stage gas turbine test facility with a degree of reaction (Λ) ranging from 0.2 to 0.6 and a blade aspect ratio (h/c) between 3 and 4 and neglects the radial tip clearance gap [32]; where the loading coefficient (ψ) is defined as the enthalpy drop divided by the mean blade speed square ($\Delta h/U_m^2$) and the flow coefficient (ϕ) is defined as the ratio of the axial velocity to the mean blade speed (C_a/U_m).

To verify the implementation of the loss models within the current work, the DC, KO, CC and AN loss models are used to construct the Smith chart as shown in Figs. 2(a)–2(d). The Smith chart has been mapped for the four stage 100 MW air turbine design at Λ, h/c and s/c of 0.5, 4 and 0.8 respectively, whilst zero tip clearance is assumed to match the original Smith chart. A good qualitative agreement is obtained as shown in Figs. 2(a)–2(d). The mapped Smith charts provide credibility of the developed design tool over a range of operating conditions. The four investigated loss models result in similar trends compared to the original Smith chart, although some deviations are observed. These differences are due to the fact that the conditions at which the original chart was generated do not perfectly match the design conditions used in the current model; for example the Smith chart was originally developed for a four stage gas turbine with a degree of reaction ranging between 0.2 to 0.6 and a blade aspect ratio ranging between 3 and 4. In the current study, the designs are investigated at a constant degree of reaction of 0.5 and an aspect ratio of 4.0. Additionally, the original Smith chart was developed based on manufacturer's data for steam and gas turbines, and hence there will be differences between the measured efficiencies and the numerical values obtained by the loss models which rely on a number of assumptions. Large deviations are observed for the Craig and Cox model, compared to the other loss models, since these correlations are evaluated at the backbone length (camber-line) compared to the chord length which is used in the rest of the models. The discrepancies in the efficiency trends obtained by the three other models (i.e., DC, KO and AN) are due to the differences in the definition of loss mechanisms and treatment for several effects including Reynolds number and compressibility. These differences will be discussed in detail in Section 5. Despite the differences between the original Smith chart and the results obtained using the loss models, it is worth noting that the results are consistent with those presented in the original papers by DC, KO, CC and AN, which confirms the right implementation of the loss models in the current analysis.

To further verify the developed models and ensure their versatility for different working fluids, the models were also cross-checked with published numerical and experimental studies for air, sCO_2 and R245fa (Tables 3–4), with power ratings between 144 kW and 10 MW. The boundary conditions of these verification cases are reported in Table 3 along with the results in Table 4. The first verification case relates to experimental data for a small-scale axial turbine, while the second relates to the design of a 10 MW sCO_2 turbine where the results from the mean-line design have been verified against CFD simulations. Finally, 440 kW & 1520 kW axial ORC turbine case-studies, operating with R245fa, are selected; Aungier loss model has been used to estimate the losses. Considering the uncertainties in the experimental data of the air turbine verification case (V1), the mean line design tool was also compared against CFD results presented in [18] for the same case to improve the reliability of the validation. A good agreement is obtained for both the design details and efficiency.

It is found that the developed model obtains a good agreement with the three selected verification cases with maximum percentage differences of 1.5% and 3.7% in the total-to-total and total-to-static efficiency respectively. Additionally, the loss breakdown predicted by the Auginer model has been verified against the loss breakdown [13] and a good agreement was achieved as presented in Table 4. Furthermore, the Smith chart has been mapped for R245fa case and compared against [13] and the same charts were obtained; for brevity these results are not included in the paper. It is worth noting that the loss model that achieves the closest match to the published data varies for each examined case studies. For example, the KO model obtains the smallest difference for the air case, but results in the largest difference for the sCO_2 and ORC cases. This is due to differences in the definition and representation of several effects which includes Reynolds number, compressibility, shock and post-expansion losses which can be expected to vary with the working fluid and boundary conditions. For example, post-expansion and clearance losses are significant for the ORC turbine (case-study V4), and it is found that the KO model overpredicts these losses compared to the other loss models. Further details will be discussed in Section 5.

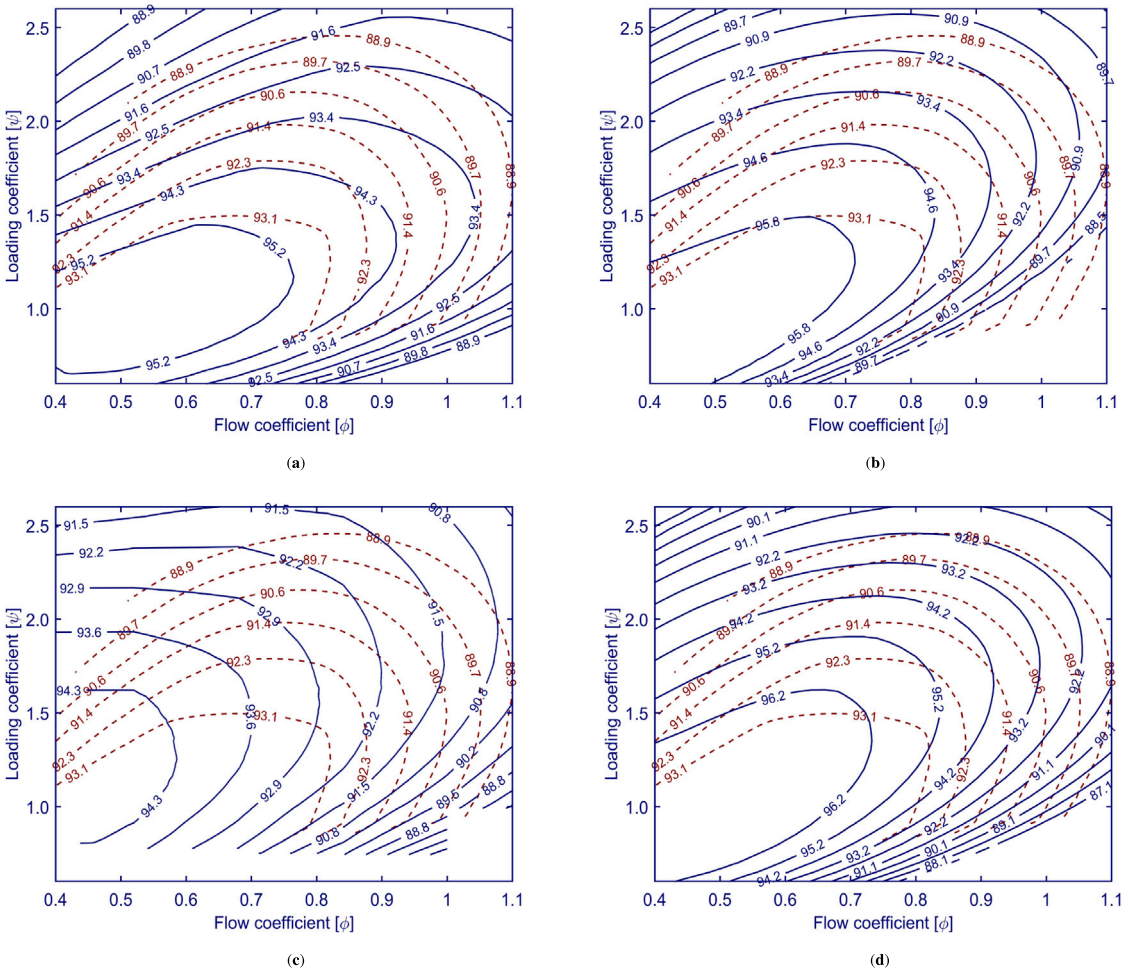

Fig. 2. Loss models verification against the original Smith chart for the 100 MW air turbine; the original Smith chart is represented by the dashed red lines and the blue solid lines represent (a) Dunham and Came (b) Kacker and Okapuu (c) Craig and Cox (d) Aungier model.

Table 3
Boundary conditions for the selected verification cases.

Parameter	Description	Unit	Case-studies serial			
			V1 [33,34]	V2 [35]	V3 [13]	V4 [13]
–	Working fluid	[–]	Air	sCO_2	R245fa	R245fa
T_{01}	Stator total inlet temperature	[K]	358.70	773.15	323.00	373.00
P_{01}	Stator total inlet Pressure	[MPa]	0.13	15.00	0.34	1.26
PR	Pressure ratio	[–]	1.25	1.55	1.70	6.40
n	Number of stages	[–]	1.00	3.00	1.00	1.00
$\dot{m}$	Mass flow rate	[kg/s]	6.79	184.00	50.00	50.00
t_{cl}	Clearance gap	[mm]	0.24	0.00	1.10	1.10
N	Rotational speed	[kRPM]	7.20	10.00	4.48	9.99
$\dot{W}$	Power output	[MW]	0.14	10.00	0.44	1.52

5. Results and discussions

The optimum turbine aerodynamic performance can be achieved at low loading and flow coefficients of approximately 0.5 and 1.0 respectively as indicated in the original Smith chart [31]. Though it is preferable to design the turbine at the optimal aerodynamic point, rotordynamic, structural, weight, life and manufacturability constraints should be considered throughout the process. As a consequence, the optimum aerodynamic design point may not satisfy the other design constraints. Thus, the mean-line design should be integrated with optimisation tools to achieve the maximum turbine efficiency along with satisfying the other design constraints. In this regard, several research studies focused on developing and optimising mean-line design tools for axial turbines operating with non-conventional working fluids [16,17,36–38].

In the current study, a generalised assessment for the Dunham and Came, Kacker and Okapuu, Craig and Cox and Aungier loss models is presented for air and non-conventional working fluids based on the operating conditions specified in Table 2. The loss model predictions are assessed over a wide range of loading and flow coefficients as recommended by Smith [31]. Furthermore, the sensitivity of the loss models to the aspect ratio and the pitch-to-chord ratio is highlighted in Section 5.6.

5.1. Large scale designs across a range of flow coefficients

In the following set of results, Figs. 3(a)–3(e), the total-to-total efficiency is predicted for the large-scale axial turbines designs where ψ, Λ, t/o have been set to 1.00, 0.50 and 0.05 respectively, while ϕ is varied from 0.4 to 1.1. Each case is further examined by considering the loss breakdown ($Y_{breakdown}$) predicted by the DC, KO, CC and AN models, at $\phi_1 = 0.5$ and $\phi_2 = 0.7$; ϕ_1 is the expected optimum design point while ϕ_2 is selected to depict the changes in the predicted loss breakdown at a high flow coefficient. The loss breakdown ($Y_{breakdown}$) value is obtained based on the pressure loss coefficient (Y) obtained by each loss model for the different types of losses (see Table 5).

Table 4
Verification results of the axial turbine design for air and sCO_2 and ORC turbines.

Parameter	Description	Loss models				
		DC	KO	CC	Aungier	Reference [13,33–35]
Case-study – V1						
ζ_N (%)	Nozzle kinetic energy loss coefficient	0.065	0.068	0.065	0.062	0.038
ζ_R (%)	Rotor kinetic energy loss coefficient	0.078	0.078	0.076	0.074	0.091
η_{t_t} (%)	Total-to-total efficiency	0.926	0.924	0.926	0.928	0.916
Difference (%)	η_{tt}(%) with respect to Exp.Data	0.983	0.873	1.100	1.310	–
Case-study – V2/[1st turbine stage]						
ζ_N (%)	Nozzle kinetic energy loss coefficient	0.058	0.047	–	0.037	–
ζ_R (%)	Rotor kinetic energy loss coefficient	0.086	0.089	–	0.072	–
η_{t_t} (%)	Total-to-total efficiency	0.904	0.902	–	0.920	0.916
Difference (%)	η_{tt}(%) with respect to Exp.Data	1.310	1.529	–	0.437	–
Case-study – V3						
Y_p	Profile loss	0.037	0.029	0.061	0.034	0.031
Y_s	Secondary flow loss	0.091	0.092	0.054	0.061	0.061
Y_{TE}	Trailing edge losses	0.013	0.017	0.010	0.017	0.017
Y_k	Clearance loss	0.072	0.092	0.076	0.072	0.071
Y_T	Total loss	0.169	0.229	0.199	0.183	0.180
η_{t_s} (%)	Total-to-static efficiency	0.901	0.879	0.889	0.896	0.891
Difference (%)	η_{ts}(%) with respect to Exp.Data	1.12	1.347	0.224	0.561	–
Case-study – V4						
Y_p	Profile loss	0.038	0.027	0.089	0.036	0.029
Y_s	Secondary flow loss	0.263	0.163	0.193	0.099	0.105
Y_{TE}	Trailing edge losses	0.046	0.019	0.011	0.011	0.012
Y_{shock}	Shock loss	–	0.012	0.000	0.023	0.024
Y_k	Clearance loss	0.139	0.229	0.101	0.139	0.139
Y_{PE}	Post-expansion loss	0.235	0.200	0.081	0.138	0.135
Y_T	Total loss	0.560	0.645	0.475	0.446	0.444
η_{t_s} (%)	Total-to-static efficiency	0.839	0.823	0.857	0.865	0.855
Difference (%)	η_{ts}(%) with respect to Exp.Data	1.871	3.743	0.234	1.169	–

For the air turbine, Fig. 3(a), it is evident that the dashed blue lines, which represent the efficiency estimated by the CC model when the Reynolds number (*Re*) is obtained based on the throat opening, deviate from the predictions of the other loss models. Given that the other loss models determine *Re* based on the chord length, using the throat opening results in a reduced *Re* by approximately half or less. This results in significantly larger Reynolds number correction factors and secondary and profile flow loss predictions that are almost double those obtained by the AN and KO models. To alleviate the throat opening effect on *Re* for the 100 MW air turbine, *Re* was obtained based on the backbone length; where the backbone length is calculated by assuming the blade mean-line can be constructed by a circular arc from the inlet to the throat, and then by a straight line to the outlet [39].

Though closer predictions are obtained by the CC when *Re* was obtained based on the backbone length, the CC model over predicts both profile and secondary flow losses as shown in Fig. 3(b). The preliminary profile and secondary flow losses, excluding both Reynolds number correction factor and compressibility effects, denoted $\overline{Y_p}$ & $\overline{Y_s}$ respectively, are presented for the various models in Figs. 4(a)–4(b). The CC model over-predicts $\overline{Y_s}$ compared to the rest of the models at the optimum design point (Fig. 4(a)). Furthermore, different trends are obtained for $\overline{Y_s}$ with increasing flow coefficient over the specified range. This is due to the different methodologies used to estimate the secondary flow losses. The DC, KO and AN models obtain $\overline{Y_s}$ as a function of lift coefficient and flow angles; where increasing the flow coefficient should result in less secondary flow losses. However, the CC model predicts $\overline{Y_s}$ based on the velocity ratio between the inlet and exit conditions (inlet/exit velocity) and lift coefficient; where the velocity ratio increases with an increasing flow coefficient.

Profile loss predictions $\overline{Y_p}$ for the 100-MW air turbine are presented in Fig. 4(b). It is observed that the CC model over-estimates $\overline{Y_p}$ with respect to the DC, KO and AN models at $\phi > 0.51$. From the literature, the DC model has been found to over-estimate the overall $\overline{Y_p}$ and thus the 2/3 factor added by AN and KO was found to result in more realistic efficiencies [40].

Table 5
Loss breakdown for air and sCO_2 and ORC turbines at flow coefficients [ϕ_1] and [ϕ_2].

Parameter	Flow coefficient [ϕ_1] = 0.5				Flow coefficient [ϕ_2] = 0.7			
	DC	KO	CC	Aungier	DC	KO	CC	Aungier
100 MW air turbine								
Y_p	0.26	0.16	0.23	0.17	0.20	0.10	0.22	0.10
Y_s	0.35	0.37	0.51	0.34	0.35	0.32	0.70	0.30
Y_{TE}	0.07	0.04	0.03	0.02	0.08	0.04	0.03	0.02
Y_k	0.12	0.10	0.12	0.12	0.11	0.09	0.11	0.11
Y_{shock}	0.00	0.00	0 .00	0.00	0.00	0.05	0.00	0.09
Y_{PE}	0.00	0.00	0.00	0.00	0.01	0.02	0.01	0.01
100 MW CO_2 turbine								
Y_p	0.16	0.14	0.34	0.19	0.15	0.13	0.34	0.18
Y_s	0.42	0.95	0.76	0.67	0.41	0.87	1.02	0.65
Y_{TE}	0.07	0.08	0.04	0.04	0.08	0.08	0.05	0.04
Y_k	0.48	0.33	0.28	0.47	0.46	0.30	0.24	0.44
1 MW ORC turbine								
Y_p	0.07	0.05	0.18	0.06	0.06	0.03	0.18	0.05
Y_s	0.13	0.21	0.40	0.19	0.13	0.16	0.54	0.17
Y_{TE}	0.04	0.02	0.02	0.01	0.06	0.02	0.02	0.01
Y_k	0.24	0.35	0.32	0.23	0.21	0.29	0.25	0.19
Y_{shock}	0.00	0.03	0.00	0.09	0.00	0.16	0.00	0.39
Y_{PE}	0.14	0.14	0.05	0.08	0.23	0.51	0.12	0.13

Given that profile and secondary flow losses, as presented in Fig. 3(b), are obtained by considering the Reynolds number effects, the Reynolds number correction factors (K_{Re}) obtained by the loss models are investigated separately. Reynolds number is obtained by both AN (hence KO and DC), and CC models based on the chord and backbone length respectively as shown in Fig. 5. Consequently, it varies between 2.7 and 6.0 $\times$ 10^5 for the CC model compared to a range of 2.1 and 3.9 $\times$ 10^5 for the AN model. Furthermore, the AN and KO models define the critical *Re* in the region of $1 \times 10^5 < Re < 5 \times 10^5$ and $2 \times 10^5 < Re < 1 \times 10^6$ respectively where the K_{Re} is equivalent

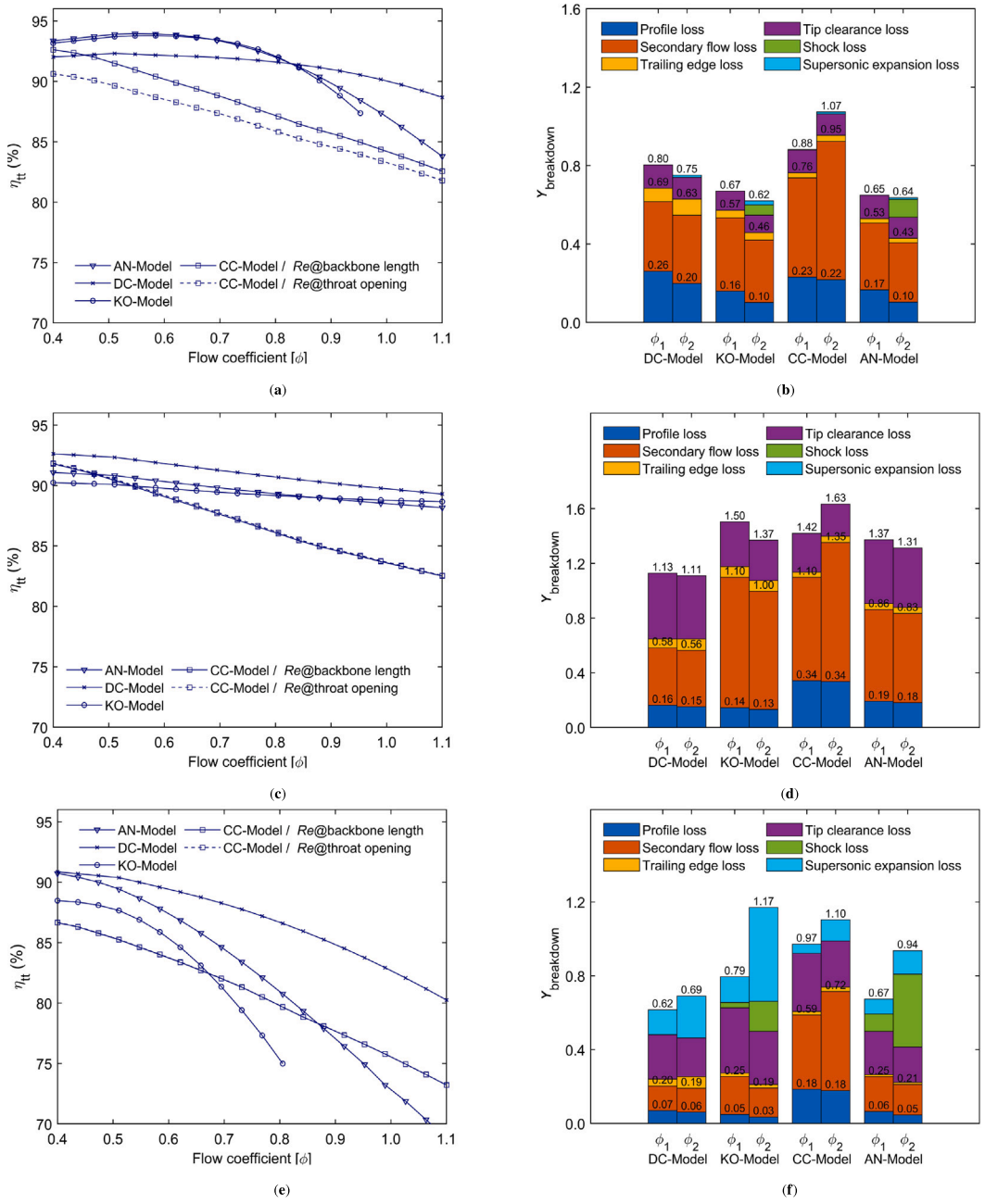

Fig. 3. Flow coefficient [ϕ] versus the total-to-total efficiency [η_{tt}] and pressure loss coefficient [Y] breakdown at flow coefficients ϕ_1 and ϕ_2 of 0.5 and 0.7 respectively for (a,b) 100 MW air turbine, (c,d) 100 MW sCO_2 turbine, (e,f) 1 MW ORC turbine.

to 1.00, while in the CC model the Reynolds number range results in a reduction in the K_{Re} from 0.85 to 0.68, as shown in Fig. 5a. This results in a reduction in the overall profile and secondary flow losses by the same factor. As for the DC model, close K_{Re} are obtained with respect to both KO and AN models. In respect to the non-conventional working fluids, $\overline{Y_p}$&$\overline{Y_s}$ experience the same increasing trends reported for the air turbine case (Figs. 4(a) & 4(b)) over the ϕ range due to their insensitivity to the working fluid properties. Nonetheless, the predictions for $\overline{Y_s}$ are closer to the other loss models for sCO_2 turbines compared to both air and ORC turbines due to the CC model sensitivity to operating at s/c ratio of 0.8 compared to 1.1 (see Section 5.6).

On the contrary, the correction factors introduced for Reynolds number and compressibility effects vary significantly with the working fluid thermodynamic properties. Calculating Re based on the throat opening, for both working fluids, result in close results to those obtained by using the backbone length. At the turbine inlet conditions, the density of R1233zd(E) and sCO_2 fluids is 138 and 116 times the density of air, and hence Re is in excess of 10^6, where a constant correction factor is obtained in the turbulent flow region for the same surface roughness to characteristic length ratio (chord/backbone length)

The Reynolds numbers and corresponding correction factors are plotted against flow coefficient for the 100.0 MW sCO_2 turbine as shown in Fig. 5b. Over a flow coefficient range of 0.4 to 1.1, Re varies between 2.2×10^7 and 9.9×10^6 for the CC model compared to a range of 1.6×10^7 to 8.4×10^6 for the AN model. Thus, a maximum K_{Re} of 0.94 is obtained for the AN model compared to 0.91 for the CC model.

Similar behaviour has been observed for the ORC turbine with higher K_{Re} due to the larger roughness to characteristic length ratio; the ORC turbine reaches a maximum backbone and chord length of 20 and 13 mm respectively in comparison to 51 and 37 mm respectively for the sCO_2 turbine. The smaller backbone length for the ORC turbine,

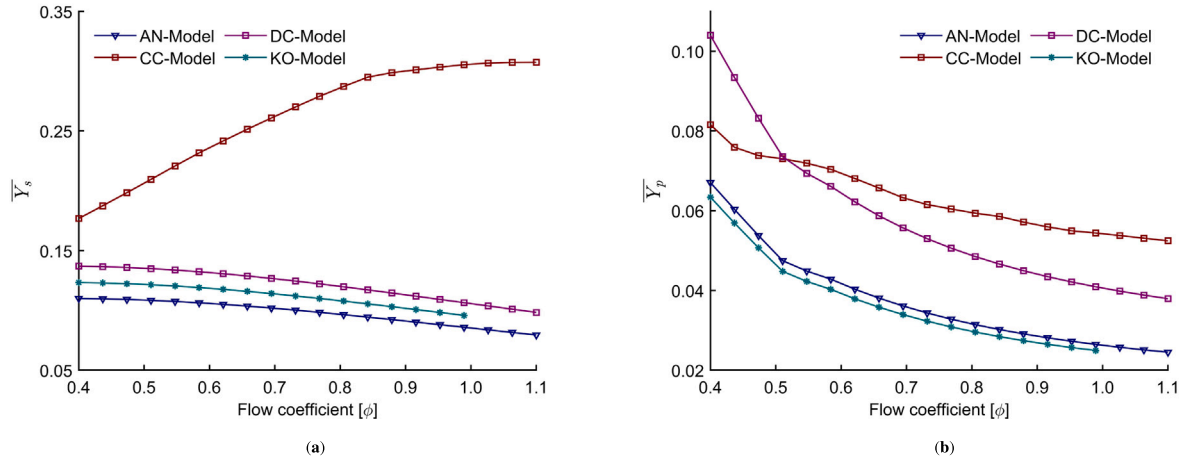

Fig. 4. Flow coefficient versus (a) the preliminary secondary flow pressure loss coefficient [$\overline{Y_s}$] for the 1st stage of 100 MW air turbine (b) the preliminary profile loss pressure loss coefficient [$\overline{Y_p}$] for the 1st stage of 100 MW air turbine.

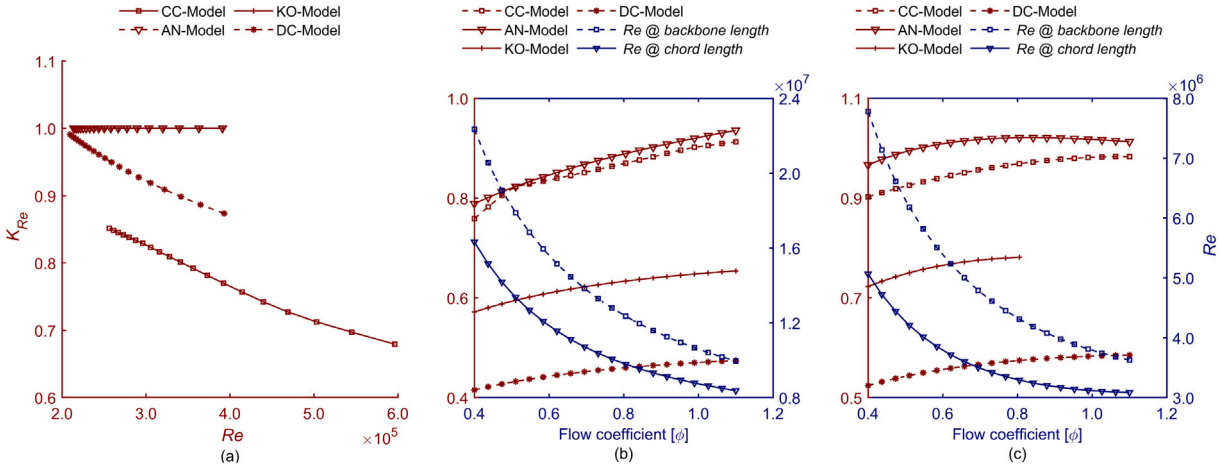

Fig. 5. (a) Reynolds number [Re] versus Reynolds number correction factor [K_{Re}] for the 1st stage of the 100 MW air turbine, flow coefficient versus [Re] and [K_{Re}] for the 1st stage of (b) 100 MW sCO_2 turbine (c) 1 MW ORC turbine.

compared to the sCO_2, results in a higher roughness to backbone length ratio and hence higher K_{Re} in the AN model with minimum and maximum values of 0.97 and 1.01 over the flow coefficient range.

In the same context, the DC model results in large efficiencies in comparison to the rest of the models for both the ORC and sCO_2 turbines (Figs. 3(c)–3(e)). The DC model implements the Reynolds number correction factor for machines operating at an average Re of 2×10^5, and also ignores surface roughness effects. Hence, small correction factors are obtained for both sCO_2 and ORC turbines as indicated in Fig. 5b & c; where Re is in the range of 10^6.

The fluid compressibility correction factor is obtained using the AN and KO models for the three working fluids as shown in Figs. 6(a) & 6(b). The ORC turbine experiences the highest compressibility effect, which results in the largest reduction in both profile and secondary flow losses with respect to the air and sCO_2 turbines owing to the high inlet Mach number. Following the ORC turbine, the air turbine experiences the second-highest compressibility effect owing to the higher Mach number at the blade inlet condition compared to sCO_2 turbine. At the turbine inlet conditions the compressibility factor of the sCO_2 and ORC turbines is equivalent to 1.05 and 0.59 respectively compared to 1.00 in air turbine.

In addition to the former effects, fluid compressibility may also result in shock losses at the leading edge of both stator and rotor blades, while supersonic expansion at the discharge of blade row could introduce supersonic expansion losses [41]. In light of the fact that sCO_2 cycles operate at low pressure ratios, and hence low expansion ratios, compared to the ORC and air turbines, it is not unexpected that they have the lowest Mach numbers at both the inlet and outlet of the blade row. Thus, they are less susceptible to the presence of shock and supersonic expansion losses at the leading edge and discharge of the blade row respectively. On the contrary, the discrepancy between the CC, DC and KO and AN loss models increases with increasing ϕ for the air and ORC cases owing to the possible presence of shock losses. It should be noted that the AN model predicts larger shock losses occurring at the leading edge compared to KO model as shown in (Figs. 3(b) & 3(f)). Moreover, the ORC turbine is found to experience large supersonic expansion losses, due to the generation of normal shock waves, and it is observed that extremely large losses are predicted by the KO model (Fig. 3(f)) if the supersonic expansion factor recommended by DC is applied to KO model.

As for the clearance loss predictions, similar tip clearance loss predictions are obtained for the air turbine relative to significant differences obtained for the sCO_2 and ORC turbines.

Owing to the significant differences in geometries obtained for the sCO_2 and ORC turbines compared to air turbines, different loss contributions are obtained for the non-conventional working fluids. In the 100 MW air turbine, secondary flow loss is the key loss mechanism at ϕ_1, contributing to the largest loss percentage of the total aerodynamic loss, followed by profile loss and tip clearance loss; contributing with 53%, 25% and 18% respectively as predicted by AN model (Fig. 3(b)).

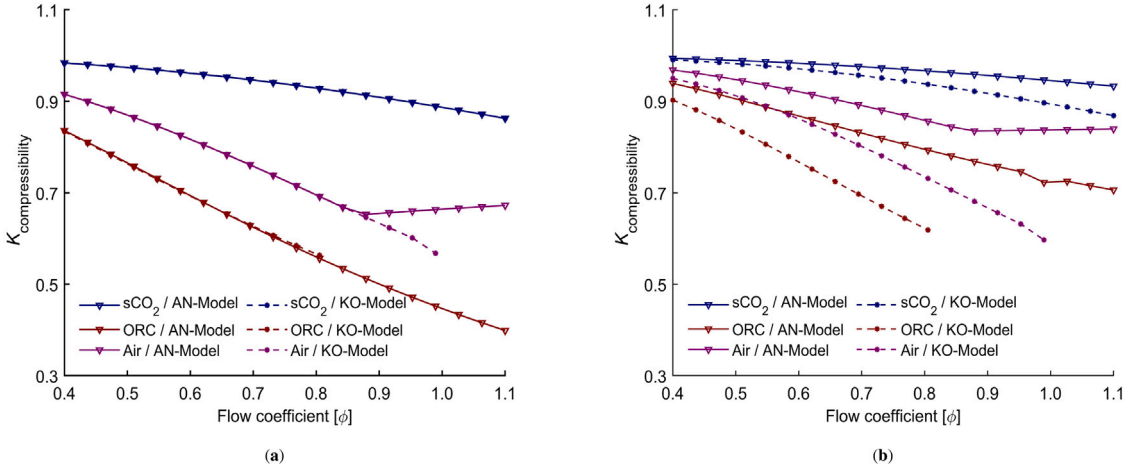

Fig. 6. Flow coefficient [ϕ] versus compressibility correction factor [K] for the 1st stage of large scale air, sCO_2 and ORC turbines by AN and KO models for (a) profile losses (b) secondary flow losses.

The other loss models resulted in the same key loss mechanisms. However, different loss distributions are obtained based the discussions provided earlier.

Based on AN model predictions, for the same turbine scale operating with sCO_2, the secondary flow loss contributes to the highest loss percentage (49%) followed by the tip clearance (34%) and profile loss (14%). Comparatively, for the ORC turbine (Fig. 3(f)), tip clearance loss was found to be contribute to the highest percentage (35%) followed by secondary flow, shock loss and supersonic expansion and profile loss accounting for 28%, 14%, 12% and 10% respectively. For both the sCO_2 and ORC turbines, the DC and KO models resulted in the same key loss mechanisms predicted by AN model at the design point of ϕ_1. However, the CC model predicts a larger contribution from secondary and profile losses and a lower contribution from tip clearance losses.

Consequently, the key loss mechanism changes with the working fluid and the implemented loss model. At the optimum aerodynamic design condition (ϕ_1), a total-to-total efficiency (η_{tt}) of 93.8%, 90.9% and 89.6% is achieved for the air, sCO_2 and ORC turbines respectively, as predicted by the AN model. The 100.0 MW air turbine achieves higher η_{tt} compared to sCO_2 turbines of the same scale due to operating at a specific speed of 0.33 compared to 0.13 for sCO_2 for the same rotational speed in addition to experiencing clearance losses approximately one-third the sCO_2 turbine for the same clearance gap (0.4 mm).

Operating at a high flow coefficient (ϕ_2) in the ORC turbine results in increase in both shock and supersonic expansion losses (Fig. 3(f)). This is due to the high Mach number experienced for ORC machines due to the large expansion ratio experienced across the turbine expansion stage alongside the low speed of sound. Hence, the ORC turbine experiences the highest sensitivity to changing ϕ, from 0.5 to 0.7, compared to both air and sCO_2 turbines; the total aerodynamic loss change by 11%, 48%, 13% and 40% for the DC, KO, CC and AN models respectively.

5.2. Large scale designs across a range of loading coefficients

To examine the predictions of the various loss models over a range of loading coefficients, ψ has been varied from 0.80 to 2.50, whilst ϕ, Λ and t/o are held constant at 0.50, 0.50, and 0.05 respectively. The total-to-total efficiency is predicted for large-scale axial turbines over the loading coefficient range for air, sCO_2 and ORC applications as shown in Figs. 7(a)–7(e). The plots are further supported with the loss breakdown predicted by the DC, KO, CC and AN loss models at ψ_1 and ψ_2 of 1 and 2 respectively (see Table 6); ψ_1 is the optimum design point while ψ_2 is selected to depict the changes in loss breakdown predicted by the various loss models at a higher loading coefficient.

Table 6
Loss breakdown for air and sCO_2 and ORC turbines at loading coefficients [ψ_1] and [ψ_2] of 1.0 and 2.0 respectively.

Parameter	Loading coefficient [ψ_1] of 1.0				Loading coefficient [ψ_2] of 2.0			
	DC	KO	CC	Aungier	DC	KO	CC	Aungier
100 MW air turbine								
Y_p	0.26	0.16	0.23	0.16	0.64	0.42	0.31	0.43
Y_s	0.35	0.37	0.51	0.34	0.57	0.69	0.55	0.60
Y_{TE}	0.07	0.04	0.03	0.02	0.1	0.04	0.03	0.02
Y_k	0.12	0.10	0.12	0.12	0.13	0.07	0.06	0.13
Y_{shock}	0.00	0.00	0 .00	0.00	0.00	0.02	0.00	0.03
Y_{PE}	0.00	0.00	0.00	0.00	0.00	0.00	0.03	0.00
100 MW CO_2 turbine								
Y_p	0.16	0.15	0.34	0.19	0.43	0.38	0.43	0.52
Y_s	0.42	0.95	0.76	0.67	0.72	1.85	0.87	1.11
Y_{TE}	0.07	0.08	0.04	0.04	0.09	0.07	0.03	0.04
Y_k	0.48	0.33	0.28	0.47				
1 MW ORC turbine								
Y_p	0.07	0.05	0.18	0.065	0.15	0.10	0.24	0.14
Y_s	0.13	0.21	0.40	0.19	0.20	0.36	0.42	0.28
Y_{TE}	0.04	0.02	0.02	0.01	0.04	0.02	0.02	0.01
Y_k	0.24	0.35	0.32	0.23	0.26	0.29	0.08	0.27
Y_{shock}	0.00	0.03	0.00	0.09	0.00	0.08	0.00	0.16
Y_{PE}	0.14	0.14	0.05	0.08	0.20	0.17	0.03	0.06

Increasing ψ over the specified range results in increase in both profile and secondary flow losses with respect to the basic case-study (ψ_1) as shown in Figs. 7(a)–7(e). Secondary flow losses are estimated as a function of the lift coefficient in all loss models where turbine designs with a higher stage loading coefficient experience higher lift coefficients, and hence higher secondary flow losses. Increasing ψ results in a higher change in the whirl velocity components across the blade row and hence result in higher profile losses [40]. For the sCO_2 turbine case, the CC model over-predicts $\overline{Y_s}$ with respect to the AN model until ψ_2 of 1.24 and then the AN model predicts higher the losses than the CC model until a maximum loading coefficient of 2.50 as shown in Fig. 8(a). Similar conclusions can be drawn for the CC model sensitivity to changing s/c ratio (Section 5.1)

The change in profile loss, excluding both Reynolds number correction factor and compressibility effects, with respect to increasing the loading coefficients is reported in Fig. 8(b) for the DC, CC and AN loss models over a varying loading coefficient from 0.80 to 2.50. At a high loading coefficient, the CC model predicts lower $\overline{Y_p}$ than the AN and KO models for the sCO_2 turbine. However, at ψ less than 1.70, different predictions are obtained with the CC model predicting high $\overline{Y_p}$ and similar to the $\overline{Y_s}$ predictions, the results are slightly different

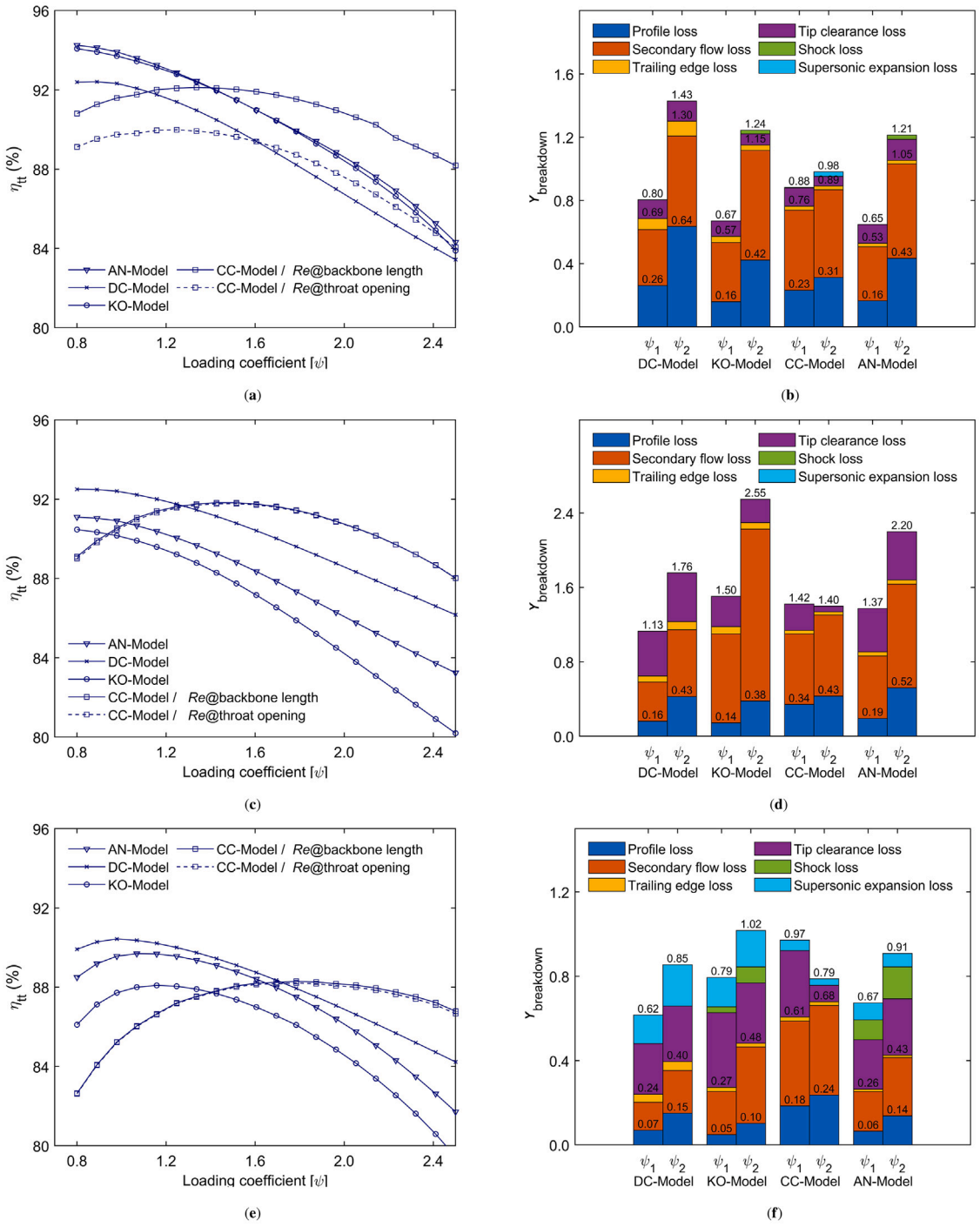

Fig. 7. Loading coefficient [ψ]versus total-total efficiency [η_{tt}] and the pressure loss coefficient [Y] breakdown at loading coefficients ψ_1 and ψ_2 of 1 and 2 respectively for (a, b) 100 MW air turbine, (c, d) 100 MW sCO_2 turbine, (e, f) 1 MW ORC turbine.

for both air and ORC turbines (see Appendix B). The Reynolds number correction factors (K_{Re}) estimated by the four loss models are obtained for all turbines; where results similar to Fig. 5 are obtained, but an increasing trend is obtained for the Reynolds number over the loading coefficient range and for brevity this figure is not included in the results section. In the 100 MW air turbine, K_{Re} ranging from 0.89 to 1.00 is estimated by AN model compared to K_{Re} ranging between 0.59 and 0.77 for the CC model which is due to the difference in the defined transition region. Increasing ψ for the sCO_2 turbine results in larger blade heights and hence larger chord and backbone lengths where the roughness effect becomes less pronounced. In both the CC and AN, and hence DC and KO models, K_{Re} decreases as the loading coefficient increases. The Reynolds number varies between 1.5 and 4.9×10^7 for the CC model compared to varying between 1.1 and 3.6×10^7 for the AN model. This results in maximum and minimum K_{Re} of 0.84 and 0.63 for CC model and 0.85 and 0.69 for AN model. Similar behaviour is obtained for ORC turbines where the CC model results in Re ranging from 5.2×10^6 to 1.8×10^7 in comparison to varying from 3.6×10^6 to 1.1×10^7 for the AN model. Similar conclusions can be drawn for the DC model predictions at high Reynolds number cases as discussed earlier in the flow coefficient case (Section 5.1). The loss breakdown for each working fluid is presented in Figs. 7(b)–7(f) & Table 6 for large scale turbines operating at ψ_1 and ψ_2 of 1 and 2 respectively. The relative change in total aerodynamic loss obtained by all loss models, due to

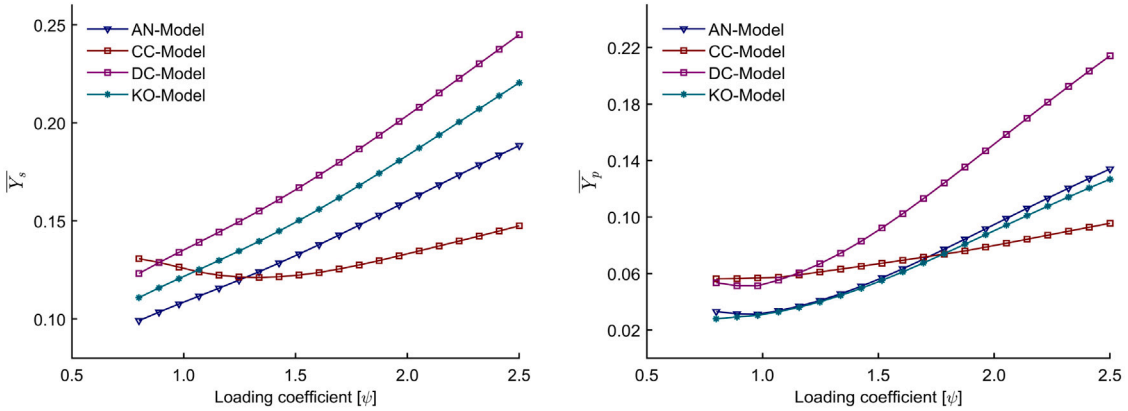

Fig. 8. Loading coefficient [ψ] versus (a) the preliminary secondary flow pressure loss coefficient [$\overline{Y_s}$] for the 1st stage of 100 MW sCO_2 turbine (b) the preliminary profile loss pressure loss coefficient [$\overline{Y_p}$] for the 1st stage of 100 MW sCO_2 turbine.

increasing ψ from 1 to 2, suggest that the air turbine is more sensitive to the loading coefficient in comparison to the sCO_2 and ORC turbines. Additionally, for all three fluids the CC model appears to be the least sensitive to changes in the loading coefficient.

5.3. Tip clearance loss for small-scale designs

Given that clearance losses are likely to contribute more significantly in small-scale turbines than in large-scale designs, this section pays particular attention to the clearance loss predictions before examining the other loss mechanisms (profile and secondary flow, etc.). In the current study, un-shrouded blades' design is considered for the developed turbines. Hence, in this set of results, only three models are examined, namely, Kacker and Okapuu, Craig and Cox and Aungier model. This is done since the Aungier implements the correlation proposed by Dunham and Came for predicting the tip clearance losses for un-shrouded blades.

In view of the fact that all of the loss correlations were developed for large-scale air turbines, where the standard clearance gap is around 1 to 2% of the average blade height [42], Figs. 9 show the loss model correlations for a wider range of clearance gap to blade height ratios that are relevant for a small-scale turbine design assuming a clearance gap up to 0.4 mm.

For the small-scale air turbine design, Fig. 9, the three models achieve very close predictions up to a clearance gap to rotor blade height ratio of 4.0%. At higher relative clearances, the models deviate significantly with large tip clearance loss coefficients being predicted by both the KO and CC models with respect to AN model. Similar conclusions can be drawn for the sCO_2 and ORC cases. Owing to the compactness of the small-scale turbine design, the tip clearance losses are highly significant due to the large clearance gap to blade height ratios. It can be concluded, that contrary to the 100-MW air turbine, the KO model and CC models over-predict the tip clearance losses with respect to the AN model for the 100 kW turbine as shown in Fig. 9a. Furthermore, the small-scale turbine design experiences a different range of the t_{cl}/h ratio owing to the compactness of the turbine design. ORC turbines experience the highest t_{cl}/h ratio (up to 33%) followed by air turbines (up to 22%) and sCO_2 (up to 14%) and hence, they experience high clearance losses compared the large-scale turbines. It is worth noting that these models estimate the tip clearance losses based on the turbine design geometry along with empirical constants that were obtained and verified for conventional and large-scale air turbines.

5.4. Small scale designs across a range of flow coefficients

In this section, the loss models are compared for the small-scale turbines with the operating conditions specified in Table 2. Considering the results discussed in Section 5.3, it is worth noting that some of the models failed to converge due to very large relative clearance gaps. Thus, for this analysis clearance losses were neglected and hence significantly high efficiencies were obtained for all turbines. This allows a full investigation into the loss model predictions for small-scale air, sCO_2 and ORC turbines with power ratings of 100 kW, 300 kW, 10 kW respectively. Similar to the large scale turbines' analysis, (Figs. 3(a)–3(e)), results are obtained for the small scale turbines, at the same design conditions, over a flow coefficient range from 0.4 to 1.1. Nonetheless, for brevity, figures are included in Appendix A and the main findings are presented in the following discussions.

Contrary to the large-scale air turbine, the KO model results in the highest efficiency for the small air turbine among all the models due to predicting lower secondary flow losses. This is due to ignoring the Reynolds number effect on the secondary flow losses. For the small-scale air turbine, the Reynolds number correction factor (K_{Re}) is more significant than for the large-scale air turbine since the Re in the order of 10^4 and thus the flow is more subjected to laminar boundary layer separations and more developed secondary flow at the end wall regions. Within the laminar flow regime, over the flow coefficient range the CC model results in a minimum and maximum K_{Re} of 1.4 and 1.8 respectively, compared to 2.0 and 2.8 for the AN model. Although the CC model results in lower K_{Re}, it results in the lowest overall efficiency since it predicts higher $\overline{Y_p}$ & $\overline{Y_s}$, as discussed in Section 5.1. Additionally, it is worth emphasising that the DC model Re holds until 5×10^4. So, operating at Re lower than the specified limit will result in rapid reduction in the efficiency compared to the actual values predicted by the model [2]. Despite the small geometry obtained for both the sCO_2 and ORC turbines, they both experience turbulent and transitional flow regimes owing to the high working fluid density. Similar to the large scale turbine designs, the CC model results in lower efficiencies compared to the other loss models for both ORC and sCO_2 due to over predicting both $\overline{Y_p}$ & $\overline{Y_s}$ (as reported in Figs. 4(a) & 4(b)). The deviation between the CC model and the other loss models is larger in small scale designs due to over estimating K_{Re} compared to the large scale turbine (Fig. 5) and hence, results in an increase in both profile and secondary by a larger factor.

For the characteristic of the flow regime effect, the small-scale ORC and sCO_2 turbines experience a similar behaviour to that experienced for the large-scale turbines, but with greater effect to the surface roughness over the flow coefficient (ϕ) range from 0.4 to 1.1. Owing to the compact design geometries of small scale turbines, the effect of

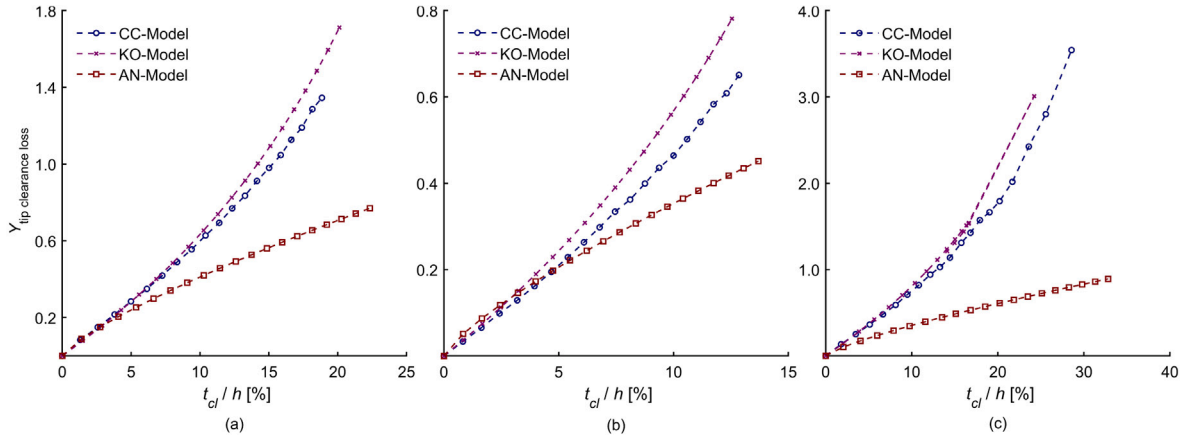

Fig. 9. Tip clearance gap [t_{cl}] to rotor blade height [h] ratio versus tip clearance pressure loss coefficient [Y] for (a) 100 kW air turbine, (b) 300 kW sCO_2 turbine and (c) 10 kW ORC turbine.

the roughness is more pronounced than in the large-scale turbines. A maximum K_{Re} of 1.65 is obtained for the small scale sCO_2 turbine using the CC model, compared to 0.91 for the large scale machine (Fig. 5). In comparison, a maximum K_{Re} of 1.20 is obtained by the AN model for the small scale design. Given that the roughness effect is not considered in DC and KO model, both models resulted in small correction factors compared to both AN and CC models.

Compared to the small-scale sCO_2 turbine, the small-scale ORC turbine results in similar Reynolds number correction factors. Over the ϕ range, K_{Re} ranges between 1.56 and 1.77 for the CC model. Whilst, the AN model results in transition flow regime for the ORC turbine with K_{Re} of 1.00. Given that shock losses are predominantly a function of expansion ratio and velocities, which are scale independent, similar conclusions are drawn for the shock and supersonic expansion losses experienced with the large scale ORC turbine (Section 5.1).

5.5. Small scale designs across a range of loading coefficients

Similar to the large scale turbines' analysis (Figs. 7(a)–7(e)), results are obtained for the small scale turbines, at the same design conditions, over a loading coefficient range from 0.80 to 2.50. Nonetheless, for brevity, the figures are included in Appendix B and the main findings are presented in the following discussions.

Similar to the results presented in Section 5.4, the KO model predicts the highest efficiency for the 100 kW air turbine over the range. Contrary to the large scale designs, presented in Section 5.2, the CC model results in close efficiency predictions to the other loss models in the sCO_2 turbine and deviates significantly from the other loss models for the ORC turbine. This is due to the differences in predicting the Reynolds number effect. In the small-scale sCO_2 turbine design, the backbone length ranges from 2.6 to 8.3 mm in comparison to 33.0 to 106.5 mm for the large-scale turbine design. This results in higher surface roughness to backbone length ratio. Thus, the maximum K_{Re} increases from around 0.84, in the large scale turbine design, to 1.43 in CC model compared to an increase from 0.85 to 1.20 in AN model.

Likewise, for the ORC turbine, the K_{Re} estimated by CC model reaches up to 1.7 owing to achieving a minimum backbone length of 1.4 mm whilst the AN model results in lower effect for surface roughness due to the defined transition zone and the larger chord length. For the ORC turbine, CC model predicts Re in the range of 5.4×10^5 to 1.8×10^6 compared to a range from 3.6×10^5 to 1.2×10^6 in AN model. Based on AN surface roughness effect should be considered at Re greater than 5.0×10^5. Hence, the ORC turbine experiences transition flow at low loading coefficient (<1.2). Considering that the ORC turbine operates at Re less than the sCO_2 turbine, DC model results in similar predictability to that obtained for the small scale air turbine. This is due to operating at Re that are close to the average Re that the DC model was developed for. Furthermore, the diversity in the DC model predictions increase post to ψ 1.7 due to ignoring the shock losses effect at the blade leading edge.

5.6. Loss model sensitivity to key geometrical design parameters

The flow coefficient (ϕ) and loading coefficient (ψ) are known to be important design variables that affect aerodynamic performance, as indicated in the Smith chart [31], but this section focuses on investigating the sensitivity of loss models to other geometrical design parameters such as the pitch-to-chord (s/c) and aspect ratios (h/c). The sensitivity is defined as the difference between the loss value at the examined condition and the design value in comparison to the design point; for example the sensitivity of the profile loss to increasing the (s/c) ratio from 0.8 to 1.1 is equivalent to:

$$Y sensitivity_{profile\ loss} = \frac{Y_{profileloss@s/c=1.1} - Y_{profileloss@s/c=0.8}}{Y_{profileloss@s/c=0.8}} \times 100 \quad (4)$$

The sensitivity of the loss models is investigated at both high and low (s/c) ratios with respect to an optimum reference of $s/c = 0.8$. The following set of results has been obtained at a fixed ψ, ϕ and Λ of 1.0, 0.5 and 0.5 respectively. The blade s/c ratio influences turbine performance by affecting both profile and secondary flow losses as presented in Figs. 10(a) - 10(d). Decreasing s/c from 0.8 to 1.1 increases the profile losses for the 100 MW air turbine by 46%, 46%, 50% for the DC, KO and AN models respectively as presented in Fig. 10(a). On the contrary, decreasing s/c to 0.5 results in an increasing trend for all loss models with the least increase obtained by the CC model (39%) for the sCO_2 turbine compared to an increase by 53%, 53%, 58% for DC, KO and AN models respectively (Fig. 10(b)).

For the secondary flow losses, the DC, KO, AN models showed no sensitivity to increasing or decreasing the s/c ratio. However, increasing s/c from 0.8 to 1.1 increases the secondary flow losses by around 25% for all fluids, while reducing the s/c to 0.5, results in a maximum reduction in the secondary flow loss of 34% as shown in Figs. 10(c) & 10(d). On this matter, increasing s/c was found to result in higher secondary flow losses in the literature [43,44].

The blade aspect ratio (h/c) influences turbine performance by affecting both tip clearance and secondary flow losses. Thus, the sensitivity of the four loss models is investigated with respect to two extreme cases with aspect ratios of 3.0 and 0.5 respectively. As presented in Fig. 11(a), increasing h/c from 1.0 to 3.0 results in a reduction in the secondary flow losses for the 100 MW air turbine by 60%, 52%, 52% and 57% for the DC, KO, CC and AN models respectively. Similar results are obtained for the other working fluids, although the DC model is found to be more sensitive to the increase in aspect ratio.

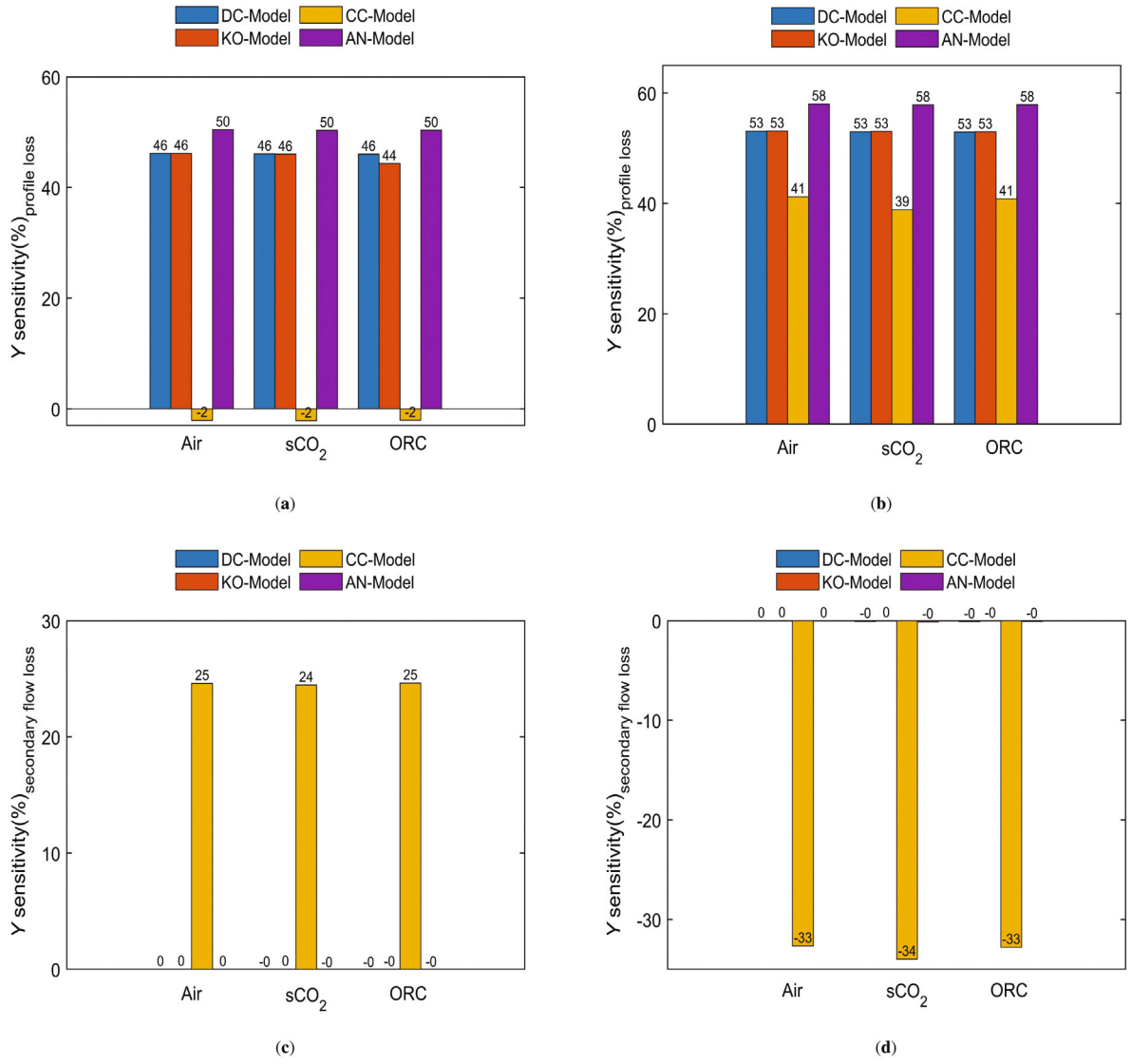

Fig. 10. The sensitivity of profile pressure loss coefficient [Y], of the 1st turbine stage of 100 MW air, 100 MW sCO_2 and 1 MW ORC turbines, to the pitch-to-chord ratio [s/c] (a) increase from 0.8 to 1.1, (b) reduction from 0.8 to 0.5, the sensitivity of secondary flow pressure loss coefficient [Y], of the 1st turbine stage of 100 MW air, 100 MW sCO_2 and 1 MW ORC turbines, to the s/c ratio (c) increase from 0.8 to 1.1 (d) reduction from 0.8 to 0.5.

On the other hand, larger differences are obtained when the aspect ratio is reduced from 1.0 to 0.5 as shown in Fig. 11(b). The AN and KO models predict lower secondary flow losses with respect to the DC and CC models; decreasing the h/c ratio from 1.0 to 0.5 for the air turbine results in an increase in the secondary flow loss by 33% and 45% in the KO and AN models, compared to 74% and 49% for the DC and CC models respectively. Although decreasing the h/c ratio results in higher secondary flow losses, the KO and model results in a reduction in the secondary flow loss by 32% for the 1 MW ORC turbine as shown in Fig. 11(b). In principle, all the loss models result in an increase in the preliminary secondary flow losses, excluding Reynolds number and compressibility correction factors, with reducing aspect ratio. Nevertheless, the KO model results in less overall secondary flow losses in the ORC turbine due to the deviation of the fluid compressibility correction factor with respect to the AN model. As noted by Aungier [6], KO model compressibility factor was corrected to prevent excessive factor values for extreme cases where axial chord to height ratio is very large.

For the ORC turbine, increasing the blade h/c ratio results in a reduction in the tip clearance loss by 21 and 20% for the DC and AN models respectively, as shown in Fig. 11(c); this is because both applied the same correlation which is a function of the clearance gap to chord length. Furthermore, the clearance loss increases with a decreasing h/c ratio from 1.0 to 0.5 (Fig. 11(d)) by 15% for the DC and AN models respectively. However, neither the CC and KO models are found to be sensitive to a variation in the aspect ratio, with maximum changes of 5% being noted.

5.7. Summary of findings for small- and large-scale turbine designs

It can be concluded that secondary flow losses appear to be the most dominant loss mechanism in the large-scale air turbine design. However, for the small-scale air turbine, a higher percentage of loss is attributed to the tip clearance loss. For the large-scale sCO_2 and ORC turbines, clearance losses contribute by a larger extent to the total aerodynamic loss compared to the large-scale air turbine. This may suggest that having accurate clearance loss models becomes more important when considering modern working fluids.

For the small-scale turbines, the characteristics of the flow regime become more significant. For air turbines, a laminar flow regime exists where flow separation is expected to occur at the leading and trailing edges of the blade suction and pressure surfaces. For the sCO_2 and ORC turbines, the surface roughness effect, with respect to the characteristic

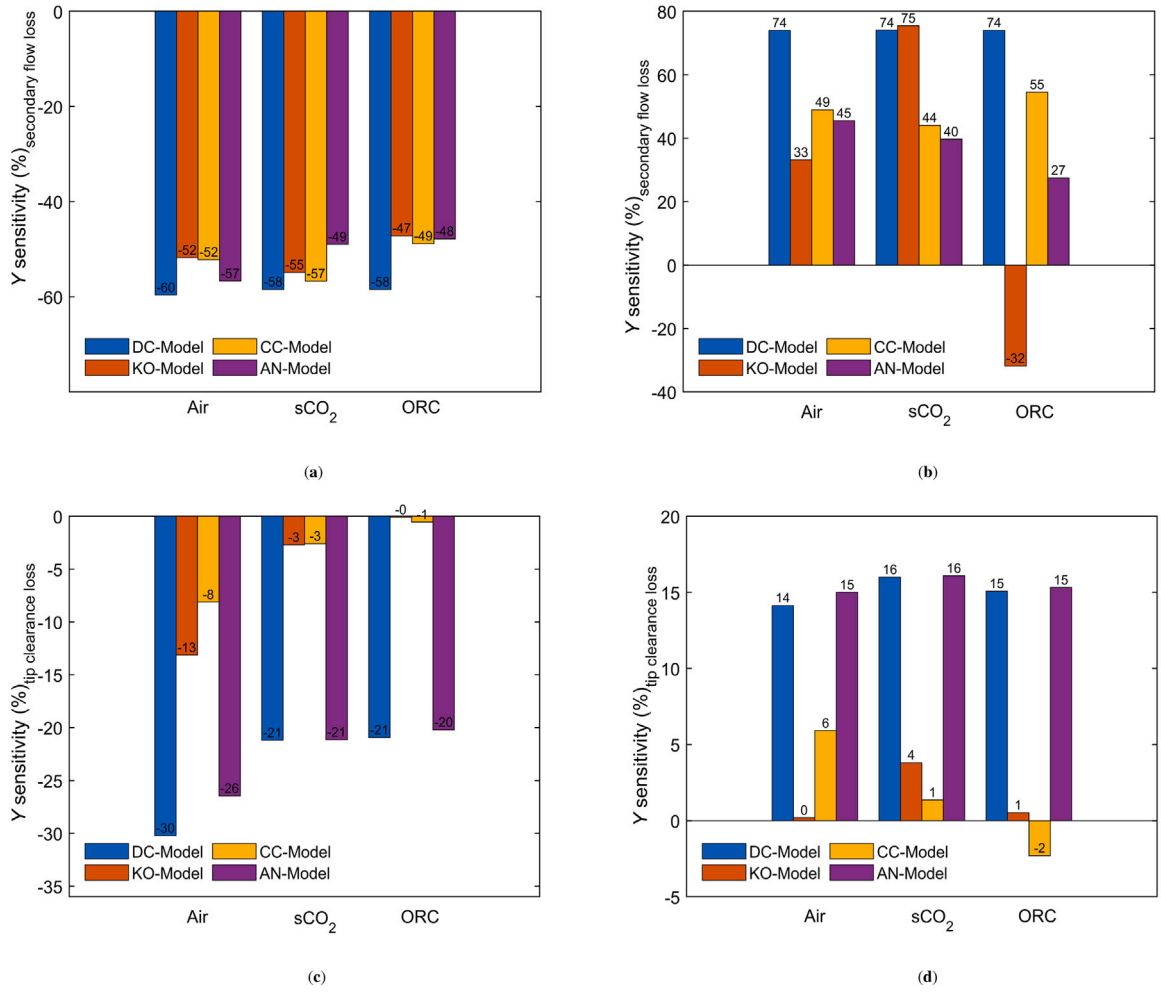

Fig. 11. The sensitivity of secondary flow pressure loss coefficient [Y], of the 1st turbine stage of 100 MW air, 100 MW sCO_2 and 1 MW ORC turbines, to the aspect ratio [h/c] (a) increase from 1 to 3 (b) reduction from 1.0 to 0.5. Sensitivity of tip clearance pressure loss coefficient, of the 1st turbine stage of 100 MW air, 100 MW sCO_2 and 1 MW ORC turbines, to [h/c] ratio (c) increase from 1.0 to 3.0 (d) reduction from 1.0 to 0.5.

length, is significant in turbulent flow regimes. Due to the compactness of small-scale turbines, in addition to the larger losses predicted by the loss models, tip clearance loss deteriorates the turbine efficiency for all working fluids, with larger effects observed in the sCO_2 and ORC turbines.

In the off-optimum design cases, ORC turbines experience the highest shock and supersonic expansion losses, and hence are a lot more sensitive to increasing the flow coefficient compared to the air and sCO_2 turbines at both design scales. For the large-scale turbine designs, the air turbine is found to be more sensitive to increasing the loading coefficient (ψ) compared to both the ORC and sCO_2 turbines. Contrary to the large-scale designs, the small-scale air and sCO_2 turbines are more sensitive to increasing ψ compared to the ORC turbine.

Given that existing loss models were developed for air turbines, the transition Reynolds number should be revised for turbines working with non-conventional working fluids. Both the ORC and sCO_2 turbines are likely to operate at higher Re compared to air turbines, and the reduction in the critical Re, due to high Mach number and surface roughness effects, is likely to affect the turbine performance; where the reduction in the critical Re would result in more significant surface roughness effects.

To conclude, to the authors knowledge, the Craig and Cox model is found to under-predict the efficiency for the non-conventional working fluids compared to the other loss models, particularly for the off-optimum design conditions and small-scale turbine designs. It is recommended to select a loss model that accounts for fluid compressibility and surface roughness effects for ORC turbines, and hence the AN model is the most suitable model in this regard. Additionally, it would be useful to use the Kacker and Okapuu model for ORC turbines if a more accurate expression for supersonic expansion losses is integrated within the model instead of the one introduced within the Dunham and Came model. Both the Kacker and Okapuu and Aungier models are found to be suitable for sCO_2 turbines considering that supersonic expansion flows are less likely to occur. Finally, the Dunham and Came model results in considerably less accurate results for both sCO_2 and ORC turbines. It is worth noting here that these conclusions should be validated against experimental data. Unfortunately, most of the existing experimental work considers turbines operating with air and steam with limited experimental data available for axial sCO_2 and ORC turbines. Therefore, experimental data for validation of turbomachinery loss models and loss breakdown is scarce. In view of this, the next step would be to conduct 3D CFD simulations to further validate the models.

6. Conclusions

This paper has presented a comprehensive investigation into the performance predictions obtained using mean-line loss models that are commonly applied to the design of axial turbines, namely the Dunham and Came, Kacker and Okapuu, Craig and Cox and Aungier models. The models were evaluated over a wide range of boundary conditions and design variables. Three different case-studies were selected for air, ORC and sCO_2 turbines and each one was evaluated at two different scales. A mean-line design methodology has been implemented and verified against the Smith chart and three case-studies from the literature

for air, sCO_2 and ORC turbines to ensure the versatility of the design tool for non-conventional working fluids. A maximum percentage difference of 1.5% and 3.7% in the total-to-total and total-to-static efficiency respectively was obtained between the developed model and the verification cases along with a good qualitative agreement with the efficiency trends of the original Smith chart.

It was found that, depending on scale and working fluid, the loss models can predict significantly different loss distributions. More specifically, a large variation in the predicted tip clearance losses were found for the small-scale designs for each working fluid. Additionally, large variations were found between the Craig and Cox and Aungier loss models with regards to the Reynolds number correction factor in the case of both laminar and turbulent flow. The large- and small-scale sCO_2 and ORC turbines were found to be the most sensitive to the effect of surface roughness on both profile and secondary flow losses owing to their compact geometries.

Furthermore, this study highlights the degree of sensitivity of the loss models to changes in the geometric input parameters such as the aspect ratio and pitch-to-chord ratio. It was found that all the loss models predict similar trends, with an increasing aspect ratio leading to a slight reduction in secondary flow losses. However, compared to the other loss models the Kacker and Okapuu model results in contradicting predictions in response to a reduction in the aspect ratio for ORC turbines. Considering the pitch-to-chord ratio, the secondary flow losses were found to be sensitive to increasing the pitch-to-chord ratio as predicted by the Craig and Cox model.

This work has provided a good insight into the diversity of the predictions of the commonly used loss models for air, sCO_2 and ORC turbines across a range of scales. Future work should conduct numerical simulations to compare the loss models predictions against CFD results to assess any uncertainty in the suitability of the loss models for non-conventional working fluids. In particular, further insight is required to evaluate existing tip clearance loss correlations for small-scale designs, and to evaluate the critical Reynolds number and roughness effects in sCO_2 and ORC turbines.

Nomenclature

AM	Ainley and Mathieson
AN	Aungier
CC	Craig and Cox
DC	Dunham and Came
KO	Kacker and Okapuu
SD	Soderberg
sCO_2	supercritical CO_2
CFD	Computational fluids dynamics
CFD	Computational fluids dynamics
ORC	organic Rankine cycle
Re	Reynolds number

Roman symbol

A	Area [m]
B_g	Gauging angle [°]
c	Chord length [m]
C_a	axial velocity [m/s]
C_L	Mean velocity
$f_{(AR)}$	Aspect ratio correction factor [–]
F_k	Efficiency debit factor [–]
Δh	Enthalpy drop [J/kg]
K	Correction factor [–]
k	Specific heat ratio [–]
k_s	Surface roughness [mm]
n_s	Specific speed [rad]
N	Rotational speed [kRPM]
N_{pi}	Corrections for incidence effect [–]
N_{pr}	Corrections for Reynolds number effect [–]
N_{pt}	Trailing edge thickness losses effect [–]
$N_{sh/b}$	Secondary loss ratio [–]
$\dot{m}$	Mass flow rate [kg/s]
M	Mach number [–]
i	Incidence angle [–]
t	Maximum blade thickness [m]
t_2	Trailing edge blade thickness [m]
t_{cl}	clearance gap [mm]
o	Throat opening [mm]
P	Pressure [MPa]
P_t	Total pressure [MPa]
PR	Pressure ratio [–]
s	Blade pitch [m]
T	Temperature [K]
U	Temperature [blade speed]
V	Relative velocity [m/s]
$X_{(pb)}$	The preliminary profile loss [–]
x_{sb}	Secondary loss ratio [–]
$\dot{W}$	Power [MW]
Y	Pressure loss coefficient [–]
$\overline{Y}$	Pressure loss coefficient excluding Reynolds number and compressibility effects [–]

Greek symbols

α	flow angle [°]
β	Blade angle [°]
ζ	Enthalpy loss coefficient [–]
η_0	Efficiency at zero clearance [%]
η	Efficiency [%]
Λ	Degree of reaction [–]
λ	Empirical factor function of the blade geometry [–]
ρ	Gas density [kg/m^3]
ϕ	Flow coefficient [–]
ψ	Loading coefficient [–]

Subscripts

hub	Blade hub
inc	Correction for off-design incidence effects
M	Correction for Mach number effects
mod	Experience factor suggested by Kacker and Okapuu
m	mean
N	Stator
P	Profile loss
PE	Post-expansion loss
R	Rotor
Re	Reynolds number
s	Secondary flow loss
$shock$	Shock loss
tip	Blade tip
t	Throat
TE	Trailing edge loss
$0rel$	Total relative
tt	total-to-total efficiency
1	Inlet condition
2	Rotor inlet condition
3	Rotor exit condition

Declaration of competing interest

The authors declare that they have no known competing financial interests or personal relationships that could have appeared to influence the work reported in this paper.

Funding

This work was supported by the European Union's Horizon 2020 research and innovation programme under grant agreement No. 814985.

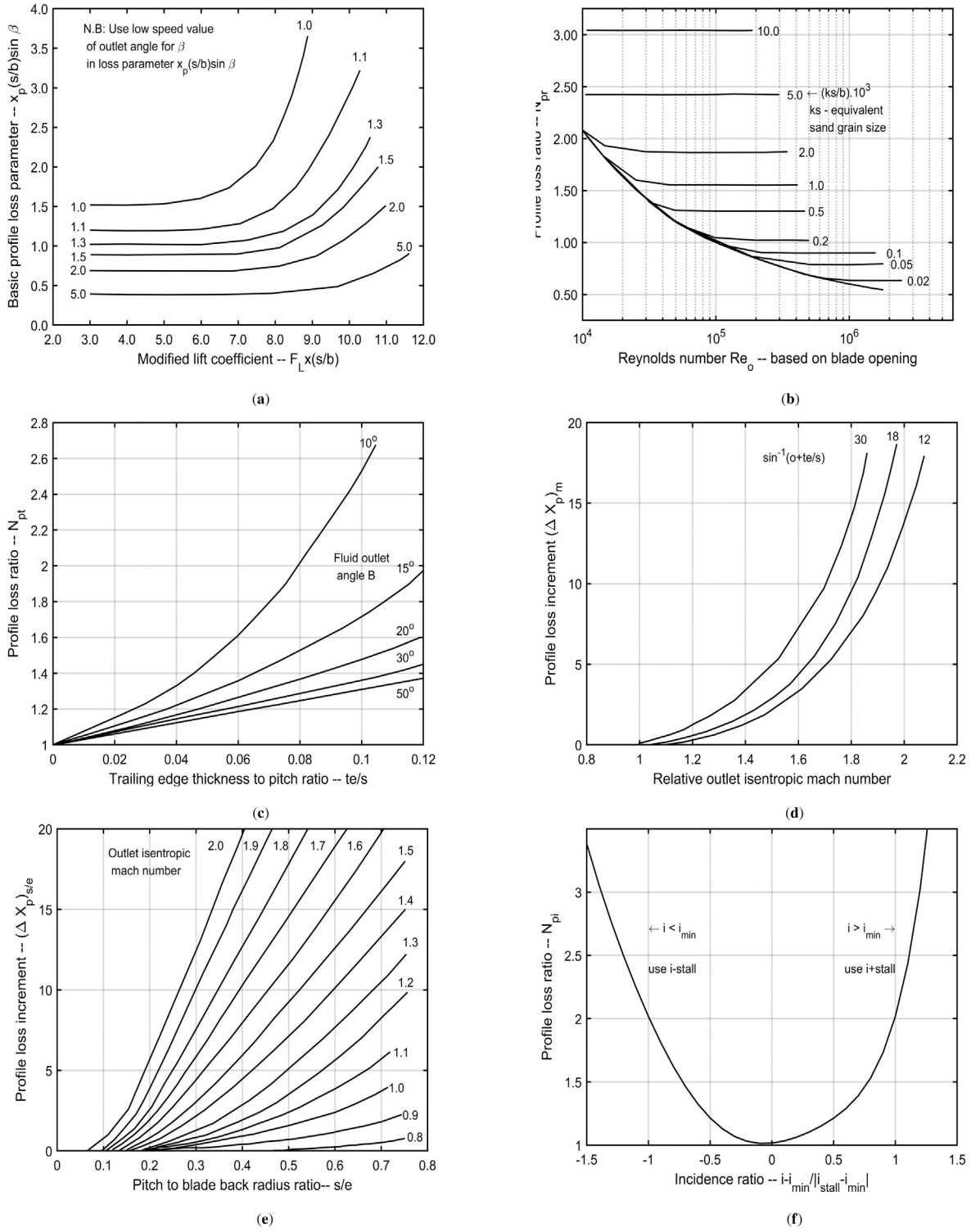

Fig. A.12. (a) Basic profile loss [3](b) profile loss ratio against Reynolds number effect,(c) trailing edge thickness losses,(d) Mach number loss for convergent blading, (e) blade back radius losses (f) uncidence losses.

Appendix A. Loss models

A full description of the loss correlations is presented in this section including loss correlations introduced by Dunham and Came, Kacker and Okapuu, Craig and Cox and Aungier loss models.

A.1. Dunham and came

Dunham and Came (DC) [4] model modified the performance correlations developed by Ainley and Mathieson (AM) [2] using updated

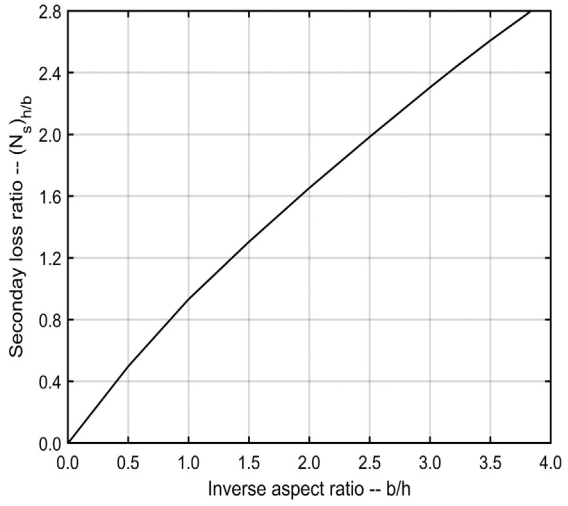

Fig. A.13. Secondary loss-aspect ratio factor.

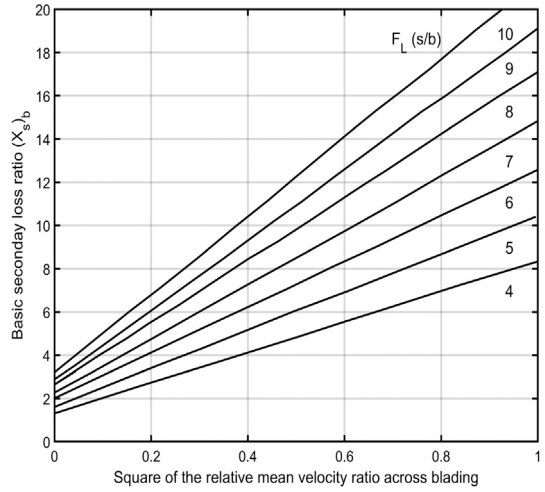

Fig. A.14. Secondary loss-basic loss factor.

experimental data and hence, expressed profile losses as follows:

$$Y_{p[AM]} = \left\{ Y_{p\ (\beta_1=0)} + \left(\frac{\beta_1}{\alpha_2}\right)^2 \left[Y_{p\ (\beta_1=\alpha_2)} - Y_{p\ (\beta_1=0)}\right] \right\} \left(\frac{t/c}{0.2}\right)^{\beta_1/\ \alpha_2} \tag{A.1}$$

$$Y_p = Y_p[AM] \times [1 + 60(M_n - 1)^2] \tag{A.2}$$

where $Y_p[AM]$ is the profile loss obtained by the AM model, M_n is the exit Mach number, For the secondary flow loss, DC modified the AM model to include a constant of 0.0334 and chord to blade height ratio (c/h)

$$Y_s = 0.0334 \left(\frac{c}{h}\right) \left(\frac{\cos\ \alpha_2}{\cos\ \beta_1}\right) \left[\frac{C_L}{s/c}\right]^2 \left[\frac{\cos^2\ \alpha_2}{\cos^3\ \alpha_m}\right] \tag{A.3}$$

where (s/c) is the pitch-to-chord ratio, (β_1 & α_2) are the blade and flow angles respectively, and (t/c) is maximum blade thickness to chord ratio. Following, DC [4] applied the *Re* correction to the profile and secondary flow losses collectively as follows:

$$(Y_p + Y_s)_{corrected} = (Y_p + Y_s)\left(\frac{Re}{2\ \times\ 10^5}\right)^{-0.2} \tag{A.4}$$

For the tip clearance loss, the DC model accounted for the power law dependence of the tip clearance (Eq. (A.5)).

$$Y_{t_{cl}} = B\left(\frac{c}{h}\right)\left[\frac{t_{cl}}{c}\right]^{0.78}\left[\frac{C_L}{s/c}\right]^2\left[\frac{\cos^2\ \alpha_2}{\cos^3\ \alpha_m}\right] \tag{A.5}$$

where $B = 0.47$ for plain tip clearance and 0.37 for shrouded blades.

A.2. Kacker and Okapuu

Kacker and Okapuu (KO) [5] further modified the DC model to include the shock losses for the subsonic Mach number as follows:

$$Y_{p,AMDC} = \left\{ Y_{p\ (\beta_1=0)} + \left|\frac{\beta_1}{\alpha_2}\right| \left(\frac{\beta_1}{\alpha_2}\right) \left[Y_{p\ (\beta_1=\alpha_2)} - Y_{p\ (\beta_{2b}=0)}\right] \right\} \left(\frac{t/c}{0.2}\right)^{\beta_1/\ \alpha_2} \tag{A.6}$$

$$Y_{Shock} = 0.75\left(f_{hub} \times Ma_{in,rel} - 0.4^{1.75}\right)\left(\frac{r_{hub}}{r_{tip}}\right)\left(\frac{P_{0rel,in} - P_{in}}{P_{0rel,out} - P_{out}}\right) \tag{A.7}$$

where P_{0rel} is the total relative pressure, P is the static pressure, Ma is Mach number, r_{hub} and r_{tip} are the hub and tip radius respectively, in, out and rel subscripts stands for the inlet, outlet conditions and the relative property respectively.

$$Y_p = 0.914\left(\frac{2}{3}Y_{p,ADMC}K_P + Y_{Shock}\right) \tag{A.8}$$

where K_P is compressbility effect correction factor.

The DC and AM models were introduced at reference *Re* of $2\ \times\ 10^5$ based on the chord and gas exit conditions. Whilst, the KO model introduced *Re* correction as follows:

$$f_{(Re)} = \begin{cases} \left(\frac{Re}{2\ \times\ 10^5}\right)^{-0.4} & Re \le\ 2\times 10^5 \\ 1.0 & 2\times 10^5 < Re < 10^6 \\ \left(\frac{Re}{10^6}\right)^{-0.2} & Re > 10^6 \end{cases} \tag{A.9}$$

The above correction is applied for the profile losses only and hence,

$$Y_p = f_{(Re)}[Y_p] \tag{A.10}$$

KO [5] introduced a refinement to the DC model including the application of correction factors $f_{(AR)}$ and K_s to account for low aspect ratio and compressibilty effects respectively.

$$Y_{s,ADMC} = 0.0334\ f_{(AR)}\left(\frac{C_L}{s/c}\right)^2\left(\frac{\cos\ \alpha_2}{\cos\ \beta_l}\right)\frac{\cos^2\ \alpha_2}{\cos^3\ \alpha_m} \tag{A.11}$$

$$f_{(AR)} = \begin{cases} \left(\frac{1-0.25\sqrt{2-h/c}}{h/c}\right) & h/c \le 2 \\ \left(\frac{1}{h/c}\right) & h/c > 2 \end{cases} \tag{A.12}$$

$$Y_s = 1.2\ Y_{s,ADMC}\ K_s \tag{A.13}$$

Trailing edge losses is expressed using an energy coefficient expression $\Delta\Phi$:

$$\Delta\Phi^2{}_{TET} = \Delta\Phi^2{}_{TET\,(\beta_1=0)} + \left|\frac{\beta_1}{\alpha_2}\right|\left(\frac{\beta_1}{\alpha_2}\right)\left[\Delta\Phi^2{}_{TET\ (\beta_1=\ \alpha_2)} - \Delta\Phi^2{}_{TET\ (\beta_1=0)}\right] \tag{A.14}$$

$$Y_{TE} = \frac{1}{1 - \Delta\Phi^2{}_{TET}} - 1 \tag{A.15}$$

For the unshrouded blades, KO introduced a new correlation for the blade rows to be:

$$\Delta\eta_{t_{cl}} = \Delta\eta_0\left(0.93 \times \frac{t_{cl}}{h\ \cos\ \alpha_2} \times \frac{r_{tip}}{r_{mean}}\right) \tag{A.16}$$

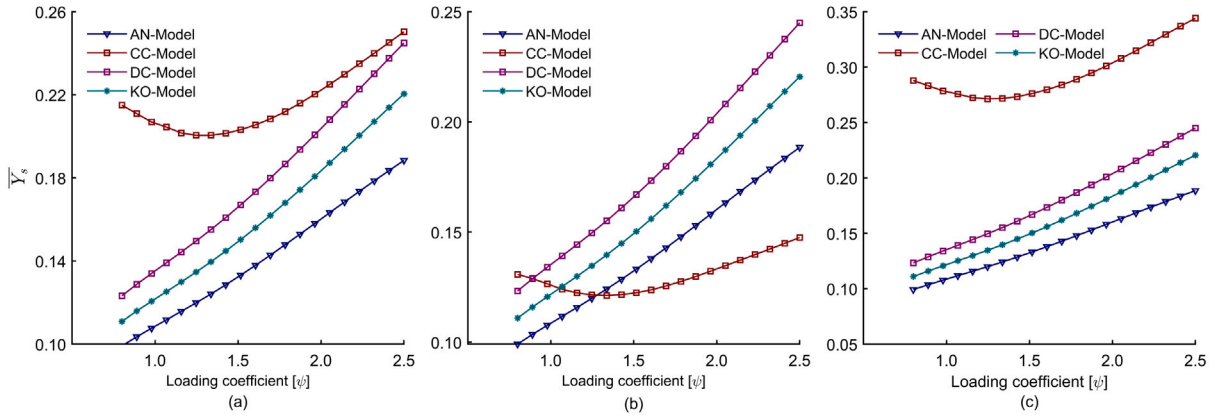

Fig. B.15. Loading coefficient [ψ] versus the preliminary secondary flow pressure loss coefficient [$\overline{Y_s}$] for the the 1st stage of **(a)** 100 MW air turbine **(b)** 100 MW sCO_2 turbine **(c)** 1 MW ORC turbine.

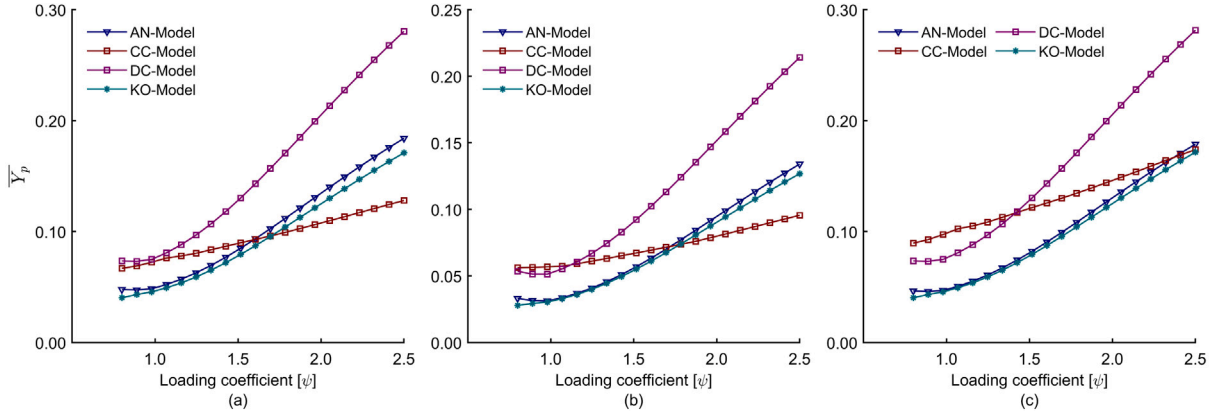

Fig. B.16. Loading coefficient [ψ] versus the preliminary profile pressure loss coefficient [$\overline{Y_p}$] for the 1st stage of **(a)** 100 MW air turbine **(b)** 100 MW sCO_2 turbine **(c)** 1 MW ORC turbine.

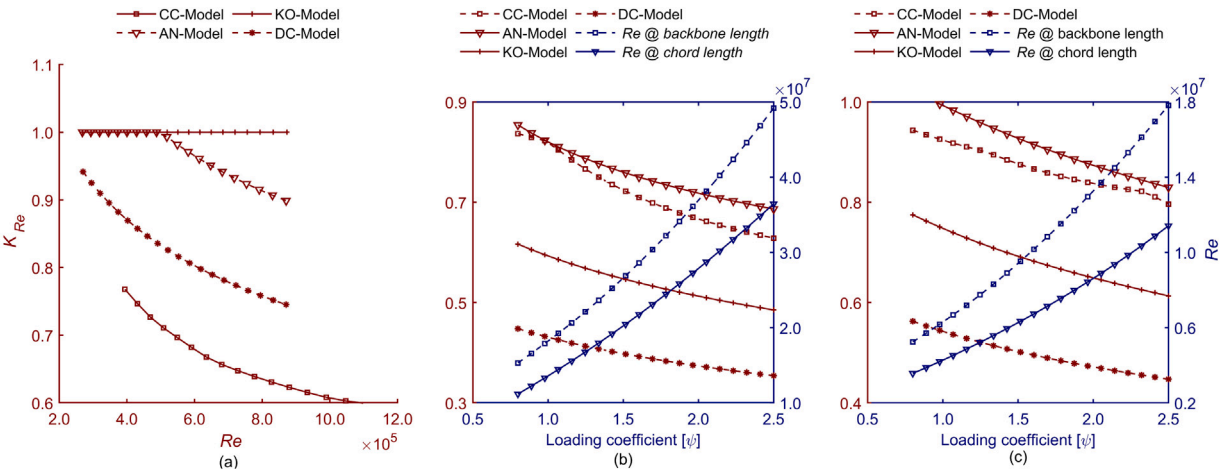

Fig. B.17. (**a**) Reynolds number [Re] versus Reynolds number correction factor [K_{Re}] for the 1st stage of 100 MW air turbine over a range of loading coefficients, loading coefficient versus [Re] and [K_{Re}] for the 1st stage of (**b**) 100 MW sCO_2 turbine (**c**) 1 MW ORC turbine.

A.3. Craig and Cox

Craig and Cox (CC) [3] introduced profile losses as a function of the preliminary profile loss $X_{(pb)}$. Followed by corrections for Re, incidence and trailing edge thickness losses effects using N_{pr}, N_{pi} and N_{pt} factors respectively.

$$X_p = x_{pb}\ N_{pr} N_{pi} N_{pt} + (\Delta x_p)_t + (\Delta x_p)_{s/e} + (\Delta x_p)_m \tag{A.17}$$

where $(\Delta x_p)_t$, $(\Delta x_p)_m$ and $(\Delta x_p)_{s/e}$ are the profile loss increments for the trailing edge thickness losses, supersonic Mach number effects for convergent blade profiles and blade back radius losses respectively. (See Fig. A.12.)

CC [3] introduced the secondary flow losses as a function of the secondary loss ratio $(N_s)_{h/b}$ and factor $(x_s)_b$. (See Figs. A.13 and A.14.)

$$X_s = (N_s)_r (N_s)_{h/b} (x_s)_b \tag{A.18}$$

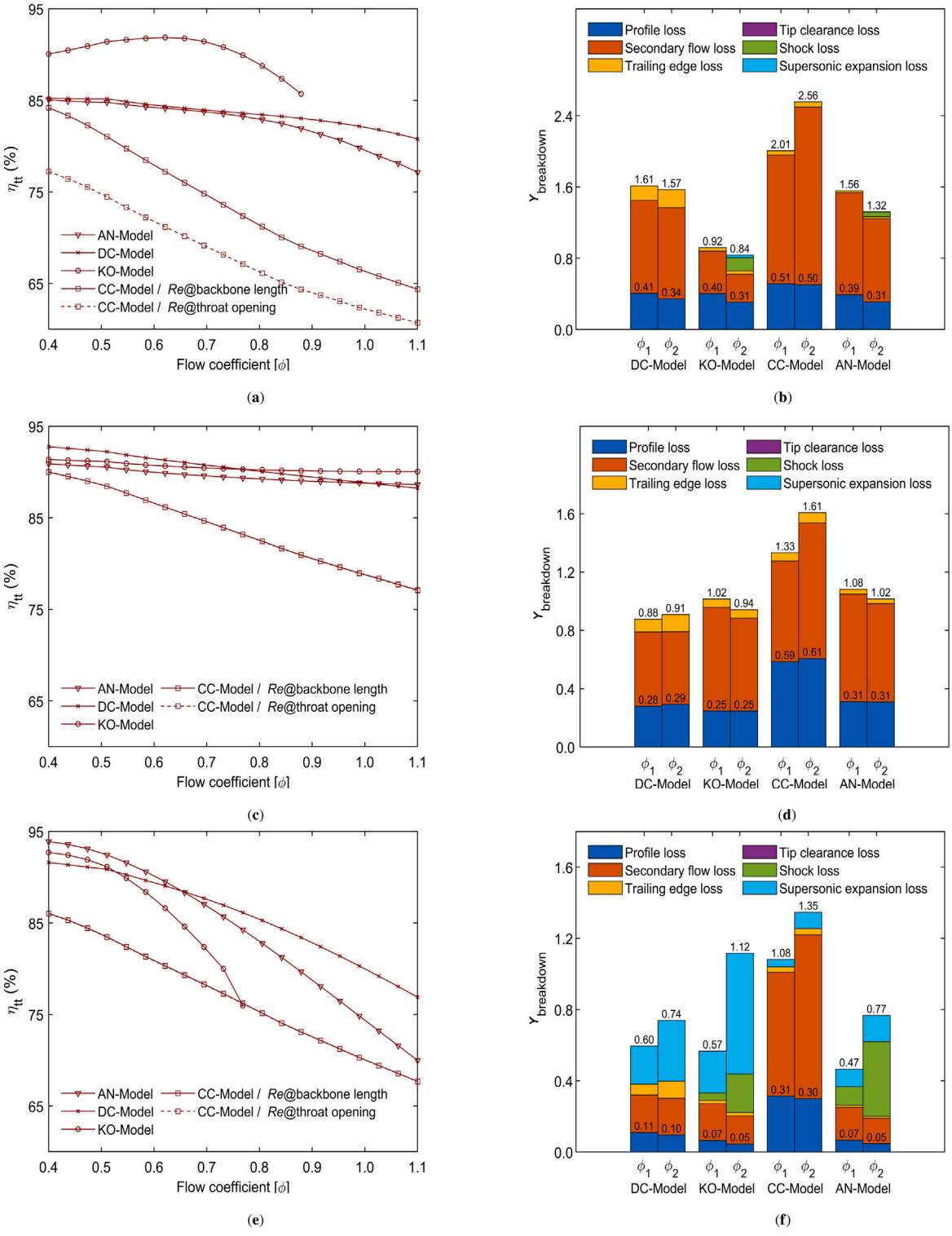

Fig. B.18. Flow coefficient [ϕ] versus total-to-total efficiency [η_{tt}] and the pressure loss coefficient [Y] breakdown at flow coefficients ϕ_1 and ϕ_2 of 0.5 and 0.7 respectively for **(a, b)** 100 kW air turbine **(c, d)** 300 kW sCO_2 turbine **(e, f)** 10 kW ORC turbine.

Eventually, the CC model presented clearance losses correlation for un-shrouded as a function of the efficiency at zero clearance (η_0), total effective area of clearance (A_k), total throat area (A_{throat}) and efficiency debit factor (F_k).

$$\Delta\eta_{t_{cl}} = \Delta\eta_0\left(1.5 \times F_k \frac{A_{t_{cl}}}{A_{throat}}\right) \tag{A.19}$$

A.4. Aungier

Aungier [6] imposed some changes on the KO model to include the roughness effect for turbulent flow regimes.

$$Y_p = K_{mod}K_{inc}K_M K_p K_{RE} \left\{\left[Y_{p1} + \left(\frac{\beta_1}{\alpha_2}\right)^2 (Y_{p2} - Y_{p1})\right](5t/c)^{\beta_1/\alpha_2} - \Delta Y_{TE}\right\} \tag{A.20}$$

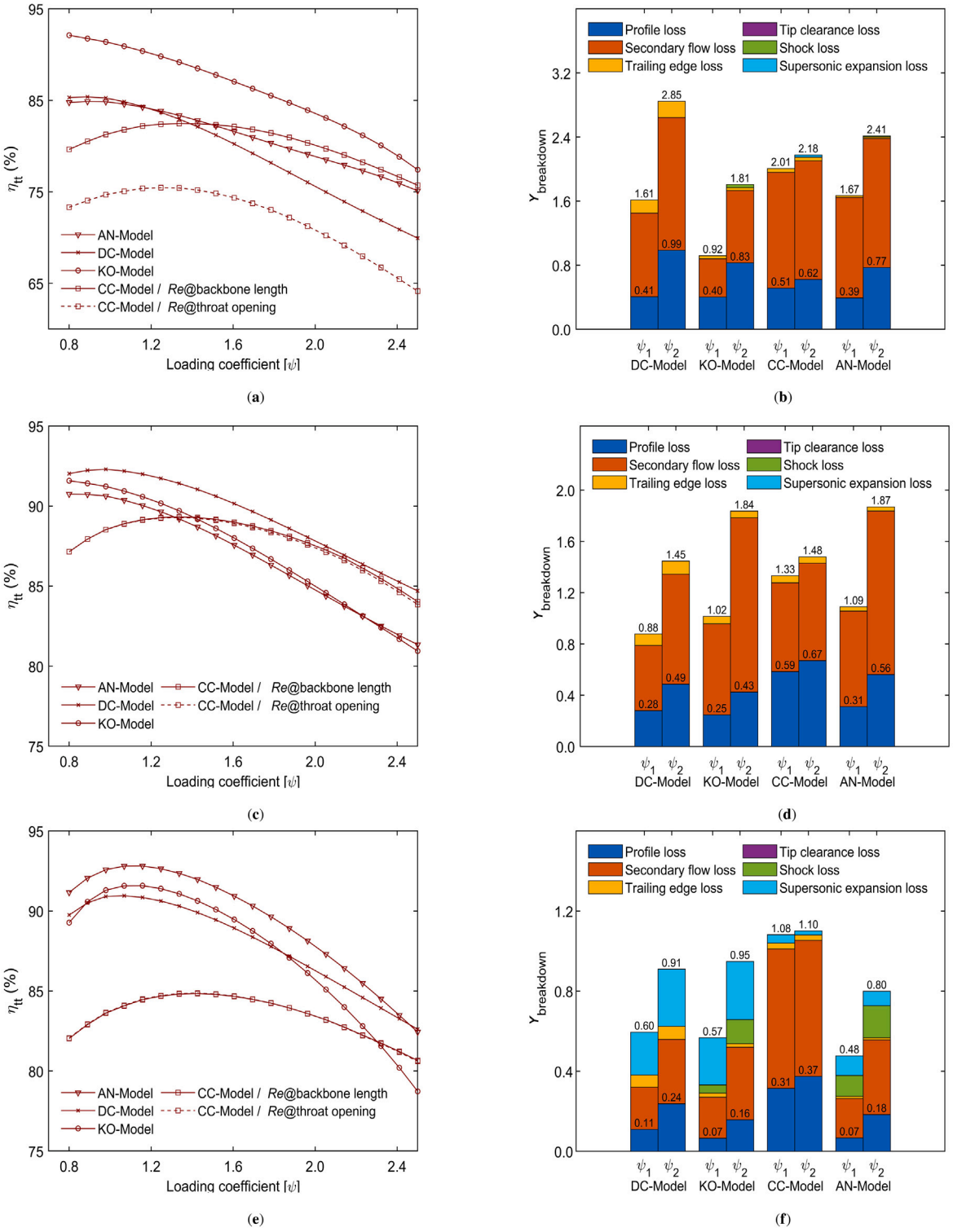

Fig. B.19. Loading coefficient [ψ]versus total-to-total efficiency [η_{tt}] and and the pressure loss coefficient [Y] breakdown at loading coefficients ψ_1 and ψ_2 of 1 and 2 respectively for **(a, b)** 100 kW air turbine **(c, d)** 300 kW sCO_2 turbine **(e, f)** 10 kW ORC turbine..

where K_{mod} is an experience factor suggested by KO, K_{inc} ,K_M, K_p and K_{RE} are correction factors for off-design incidence, Mach number, compressibility and Reynolds number effects respectively, Y_{p1} and Y_{p2} are the profile loss coefficients for nozzle blades ($\beta_1 = 0$) and rotor blades ($\beta_1 = \alpha_2$) respectively.

Aungier [6] modified the KO model correction factors for the low aspect ratio and compressibility effects and hence, expressed the secondary flow losses as follows:

$$\overline{Y}_s = 0.0334\ F_{AR}\left[\frac{C_L}{s/c}\right]^2\left(\frac{\cos\ \alpha_2}{\cos\ \beta_1}\right)\left[\frac{\cos^2\ \alpha_2}{\cos^3\ \alpha_m}\right] \tag{A.21}$$

$$F_{(AR)} = \begin{cases} (0.5\ (2c/h)^{0.7} & h/c < 2 \\ (c/h) & h/c \geq 2 \end{cases} \quad \text{(A.22)}$$

$$Y_s = K_s\ K_{Re} \sqrt{\overline{Y}_s{}^2/(1 + 7.5\overline{Y}_s)} \quad \text{(A.23)}$$

The shock loss coefficient is computed by:

$$\overline{Y}_{sh} = 0.8X_1{}^2 + X_2{}^2 \quad \text{(A.24)}$$

$$Y_{sh} = \sqrt{\overline{Y}_{sh}{}^2/(1 + \overline{Y}_{sh}{}^2)} \quad \text{(A.25)}$$

where X_1 &X_2 are parameters defined as a function of Ma number.

Supersonic expansion losses are computed as a function of the exit Mach number (M_2):

$$Y_{EX} = \left[(M_2 - 1)/M_2\right]^2 \quad \text{(A.26)}$$

Aungier computed the trailing edge loss coefficient as follows:

$$Y_{TE} = \left[t_2/s\ sin\beta_g - t_2\right]^2 = \left(\frac{t_2}{o_2 - t_2}\right)^2 \quad \text{(A.27)}$$

Where t_2 is the trailing edge blade thickness, β_g is the gauging angle, o is the throat opening. Ultimately, Aungier implements the correlation proposed by DC for predicting the tip clearance losses for un-shrouded blades (Eq. (A.5)).

Appendix B. Supplementary results

In this section, supplementary results are provided for the analysis presented in section 5. Figs. B.15 and B.16 support the results discussed in section 5.2; where the preliminary profile and secondary flow losses, excluding both Reynolds number correction factor and compressibility effects, denoted $\overline{Y_p}$ & $\overline{Y_s}$ respectively, are plotted over the investigated range of loading coefficients (See Fig. B.17).

Figs. B.18 and B.19 support the results presented in sections 5.4 and 5.5. This includes the results of the total-to-total efficiency predicted for the small-scale axial turbines over a range of flow and loading coefficients from 0.4 to 1.1 (Fig. B.18) and 0.8 to 2.5 (Fig. B.19) respectively.

References

[1] C.R. Soderberg, Gas Turbine Laboratory, Massachusetts Institute of Technology, 1949.

[2] D. Ainley, G.C. Mathieson, A method of performance estimation for axial-flow turbines, Tech. rep., Aeronautical Research Council, 1951.

[3] H.R.M. Craig, H.J.A. Cox, Performance estimation of axial flow turbines, Proc. Inst. Mech. Eng. 185 (1) (1970) 407–424, http://dx.doi.org/10.1243/PIME_PROC_1970_185_048_02.

[4] J. Dunham, P.M. Came, Improvements to the ainley-mathieson method of turbine performance prediction, J. Eng. Power 92 (3) (1970) 252–256, http://dx.doi.org/10.1115/1.3445349.

[5] S.C. Kacker, U. Okapuu, A mean line prediction method for axial flow turbine efficiency, J. Eng. Power 104 (1) (1982) 111–119, http://dx.doi.org/10.1115/1.3227240.

[6] R.H. Aungier, Turbine Aerodynamics: Axial-Flow and Radial-Flow Turbine Design and Analysis, ASME Press, 2006, http://dx.doi.org/10.1115/1.802418.

[7] E. Macchi, M. Astolfi, Chapter 9 - axial flow turbines for organic Rankine cycle applications, in: E. Macchi, M. Astolfi (Eds.), Woodhead Publishing, 2017, pp. 299–319, http://dx.doi.org/10.1016/B978-0-08-100510-1.00009-0.

[8] M.T. White, G. Bianchi, L. Chai, S.A. Tassou, A.I. Sayma, Review of supercritical CO_2 technologies and systems for power generation, Appl. Therm. Eng. 185 (2021) 116447, http://dx.doi.org/10.1016/j.applthermaleng.2020.116447.

[9] J. Lee, J.I. Lee, Y. Ahn, H. Yoon, Design methodology of supercritical CO_2 brayton cycle turbomachineries, in: Turbo Expo: Power for Land, Sea, and Air, Vol. 44717, American Society of Mechanical Engineers, 2012, pp. 975–983, http://dx.doi.org/10.1115/GT2012-68933.

[10] O.E. Balje, R.L. Binsley, Axial turbine performance evaluation. Part A—Loss-geometry relationships, J. Eng. Power 90 (4) (1968) 341–348, http://dx.doi.org/10.1115/1.3609211.

[11] J. Schmitt, R. Willis, D. Amos, J. Kapat, C. Custer, Study of a supercritical CO_2 turbine with TIT of 1350 K for Brayton cycle with 100 MW class output: aerodynamic analysis of stage 1 vane, Proc. ASME Turbo Expo 3 (2014) http://dx.doi.org/10.1115/GT2014-27214.

[12] S.I. Salah, M.A. Khader, M.T. White, A.I. Sayma, Mean-line design of a supercritical CO_2 micro axial turbine, Appl. Sci. 10 (15) (2020) http://dx.doi.org/10.3390/app10155069.

[13] L. Da Lio, G. Manente, A. Lazzaretto, New efficiency charts for the optimum design of axial flow turbines for organic Rankine cycles, Energy 77 (2014) 447–459, http://dx.doi.org/10.1016/j.energy.2014.09.029.

[14] L. Talluri, G. Lombardi, Simulation and design tool for ORC axial turbine stage, Energy Procedia 129 (2017) 277–284, http://dx.doi.org/10.1016/j.egypro.2017.09.154.

[15] L. Da Lio, G. Manente, A. Lazzaretto, Predicting the optimum design of single stage axial expanders in ORC systems: Is there a single efficiency map for different working fluids? Appl. Energy 167 (2016) 44–58, http://dx.doi.org/10.1016/j.apenergy.2016.01.020.

[16] R. Agromayor, L.O. Nord, Preliminary design and optimisation of axial turbines accounting for diffuser performance, Int. J. Turbomach. Propul. Power 4 (3) (2019) http://dx.doi.org/10.3390/ijtpp4030032.

[17] A. Meroni, J.G. Andreasen, G. Persico, F. Haglind, Optimisation of organic rankine cycle power systems considering multistage axial turbine design, Appl. Energy 209 (2018) 339–354, http://dx.doi.org/10.1016/j.apenergy.2017.09.068.

[18] A. Meroni, A. La Seta, J.G. Andreasen, L. Pierobon, G. Persico, F. Haglind, Combined turbine and cycle optimization for organic Rankine cycle power systems—Part a: turbine model, Energies 9 (5) (2016) doi:https://www.mdpi.com/1996-1073/9/5/313.

[19] A.S. Lebedev, K.S. V., Trends in increasing gas-turbine units efficiency, Thermal Eng. Soc. 55 (6) (2008) 461–468, http://dx.doi.org/10.1134/S0040601508060037.

[20] J. Lujan, J. Serrano, V. Dolz, J. Sanchez, Model of the expansion process for R245fa in an organic Rankine cycle (ORC), Appl. Therm. Eng. 40 (2012) 248–257, http://dx.doi.org/10.1016/j.applthermaleng.2012.02.020.

[21] M.T. White, A.I. Sayma, A generalised assessment of working fluids and radial turbines for non-recuperated subcritical organic Rankine cycles, Energies 11 (4) (2018) 1–26, http://dx.doi.org/10.3390/en11040800.

[22] Y. Ahn, S.J. Bae, M. Kim, S.K. Cho, S. Baik, J.I. Lee, J.E. Cha, Review of supercritical CO_2 power cycle technology and current status of research and development, Nuclear Eng. Technol. 47 (6) (2015) 647–661, http://dx.doi.org/10.1016/j.net.2015.06.009.

[23] H. Saravanamuttoo, G. Rogers, H. Cohen, Chapter 7—Axial and radial flow turbines, in: H. Saravanamuttoo, G. Rogers, H. Cohen (Eds.), Gas Turbine Theory, 5th Edition, Prentice Hall, UK, 2001, pp. 305–366, doi:https://books.google.com.eg/books?id=ummg5F227WoC.

[24] O.P. Sharma, T.L. Butler, Predictions of endwall losses and secondary flows in axial flow turbine cascades, J. Turbomach. 109 (2) (1987) 229–236, http://dx.doi.org/10.1115/1.3262089.

[25] K.W. Van Treuren, T. Simon, M. von Koller, A.R. Byerley, J.W. Baughn, R. Rivir, Measurements in a turbine cascade flow under ultra low Reynolds number conditions, J. Turbomach. 124 (1) (2002) 100–106, http://dx.doi.org/10.1115/1.1415736.

[26] J. Choi, S. Teng, J.-C. Han, F. Ladeinde, Effect of free-stream turbulence on turbine blade heat transfer and pressure coefficients in low Reynolds number flows, Int. J. Heat Mass Transfer 47 (14) (2004) 3441–3452, http://dx.doi.org/10.1016/j.ijheatmasstransfer.2004.01.015.

[27] F. Satta, D. Simoni, M. Ubaldi, P. Zunino, F. Bertini, Profile and secondary flow losses in a high-lift LPT blade cascade at different Reynolds numbers under steady and unsteady inflow conditions, J. Therm. Stresses 21 (2012) 483–491, http://dx.doi.org/10.1007/s11630-012-0572-z.

[28] R. Brachmanski, R. Niehuis, Mach number distribution and profile losses for low pressure turbine profiles with high diffusion factors, J. Turbomach. 139 (2017) http://dx.doi.org/10.1115/1.4036436.

[29] C. Prakash, D. Cherry, H. Shin, J. Machnaim, L. Dailey, R. Beacock, D. Halstead, A. Wadia, S. Guillot, W. Ng, Effect of loading level and distribution on LPT losses, in: Turbo Expo: Power for Land, Sea, and Air, Vol. 43161, 2008, pp. 917–925, http://dx.doi.org/10.1115/GT2008-50052.

[30] A.L. Braslow, A review of factors affecting boundary-layer transition, Langley Research Center, University of Virginia, Washington, DC, 1965.

[31] S.F. Smith, A simple correlation of turbine efficiency, J. R. Aeronaut. Soc. 69 (655) (1965) 467–470, http://dx.doi.org/10.1017/S0001924000059108.

[32] S. Dixon, C. Hall, Chapter 4 - axial-flow turbines: mean-line analysis and design, in: S. Dixon, C. Hall (Eds.), Fluid Mechanics and Thermodynamics of Turbomachinery, Sixth Edition, Butterworth-Heinemann, Boston, 2010, pp. 97–141, http://dx.doi.org/10.1016/B978-1-85617-793-1.00004-3.

[33] G. Groschup, Strömungstechnische Untersuchung Einer Axialturbinenstufe im Vergleich zum Verhalten der Ebenen Gitter Ihrer Beschaufelung, 1977.

[34] C. Hirsch, J. Denton, Through flow calculations in axial turbomachines, AGARD Advisory Report N.175; Technical Report; AGARD, Propulsion and Energetics Panel, Working Group 12: Neuilly Sur Seine, France, 1981.
[35] D. Shi, L. Zhang, Y. Xie, D. Zhang, Aerodynamic design and off-design performance analysis of a multi-stage sCO_2 axial turbine based on solar power generation system, Appl. Sci. 9 (4) (2019) http://dx.doi.org/10.3390/app9040714.
[36] A. La Seta, A. Meroni, J.G. Andreasen, L. Pierobon, G. Persico, F. Haglind, Combined turbine and cycle optimisation for organic Rankine cycle power systems—Part B: application on a case study, Energies 9 (2016) http://dx.doi.org/10.3390/en9060393.
[37] G.L. Martins, S.L. Braga, S.B. Ferreira, Design optimization of partial admission axial turbine for ORC service, Appl. Therm. Eng. 96 (2016) 18–25, http://dx.doi.org/10.1016/j.applthermaleng.2015.09.041.
[38] G. Morgese, M. Torresi, B. Fortunato, S.M. Camporeale, Optimised aerodynamic design of axial turbines for waste energy recovery, Energy Procedia 82 (2015) 194–200, http://dx.doi.org/10.1016/j.egypro.2015.12.019.
[39] G. Lozza, A comparison between the Craig-Cox and the Kacker-Okapuu methods of turbine performance prediction, Meccanica 17 (4) (1982) 211–221.
[40] J.D. Coull, H.P. Hodson, Blade loading and its application in the mean-line design of low pressure turbines, J. Turbomach. 135 (2012) http://dx.doi.org/10.1115/1.4006588.
[41] A. Giuffre', M. Pini, Design guidelines for axial turbines operating with non-ideal compressible flows, J. Eng. Gas Turbines Power 143 (2021) http://dx.doi.org/10.1115/1.4049137.
[42] J. Moore, J.S. Tilton, Tip leakage flow in a linear turbine cascade, J. Turbomach. (1988) http://dx.doi.org/10.1115/1.3262162.
[43] A. Perdichizzi, V. Dossena, Incidence angle and pitch–chord effects on secondary flows downstream of a turbine cascade, J. Turbomach. 115 (3) (1993) 383–391, http://dx.doi.org/10.1115/1.2929265.
[44] V. Dossena, G. D'Ippolito, E. Pesatori, Stagger angle and pitch-chord ratio effects on secondary flows downstream of a turbine cascade at several off-design conditions, J. Turbomach. (2004) 1429–1437, http://dx.doi.org/10.1115/GT2004-54083.